Stability of plane Couette flow of Carreau fluids past a deformable solid at arbitrary Reynolds numbers

Velidanda S. Tanmay,[1,2] Ramkarn Patne,[2] and V. Shankar[2,a)]
[1)] *Department of Chemical Engineering, BITS, Pilani, Goa Campus, Goa 403726, India*
[2)] *Department of Chemical Engineering, Indian Institute of Techology, Kanpur 208016, India*

The linear stability of plane Couette flow of both power-law and Carreau fluids past a deformable, neo-Hookean solid is analyzed at arbitrary Reynolds numbers. An algebraic error in the mathematical formulation of the earlier studies (for the power-law fluid) is corrected and is shown to result in quantitative differences in the predictions for the stability of the flow. Due to the lack of a proper (zero-shear) viscosity scale and a timescale for onset of shear thinning in the power-law model, we show that the stability analysis of the flow yields vastly different scalings for the unstable mode depending on the way the problem is scaled to render it dimensionless. When the deformable solid properties are used to non-dimensionalize, we show that for the unstable modes (so-called 'wall modes' at high Re) $\Gamma_c \propto Re^{\frac{-1}{(2n+1)}}$, while when flow properties are used to non-dimensionalize, $\Gamma_c \propto Re^{\frac{-1}{3}}$ much akin to a Newtonian fluid, where $\Gamma = V_m^* \eta^* / G^* R^*$ is the dimensionless shear rate in the flow, and Γ_c denotes the minimum value required for instability. Here, V_m^* is the velocity of the top plate, G^* is the shear modulus of the solid, R^* is the fluid thickness and η^* is the (arbitrary) viscosity scale in the power-law model. Within the framework of the power-law model, it is not possible to discriminate between the two predicted scalings. To resolve this in an unambiguous manner, we used the Carreau model to account for shear thinning and to study its role on the stability of flow past deformable solid surfaces. The Carreau model has a well-defined zero-shear viscosity η_0^* as well as a timescale λ^* that characterizes the onset of shear thinning. For fixed $\lambda^* \eta_0^* / (\rho^* R^{*2})$, we show that the unstable wall modes scale as $\Gamma_c \sim Re^{\frac{(1-2n)}{3}}$ at high Re, thus providing a resolution to the ambiguity in the results obtained using the power-law model. The present work thus shows that, at moderate to high Re, shear thinning has a strongly stabilizing effect on the wall mode instability in flow past deformable solid surfaces.

[a)] Author for correspondence; E-mail: vshankar@iitk.ac.in

I. INTRODUCTION

The stability of fluid flow past deformable solid surfaces has garnered much attention in the last decade, from both experimental and theoretical standpoints. The motivation for these studies stems both from biological settings[1] as well as microfluidic applications[2] that use soft elastomeric platforms in their design. However, much of the focus was restricted to the flow of Newtonian fluids past deformable surfaces. There are many instances where the non-Newtonian nature of the fluid could become relevant to the instability of the flow. This is particularly the case for biological fluids such as blood, saliva and synovial fluid. Even microfluidic applications often involve the flow of solutions of biopolymers which also exhibit non-Newtonian effects. The experimental findings by Krindel and Silberberg[3] of an early onset to turbulence at a Reynolds number (Re) ≈ 600 for flow through a gel-walled tube provided perhaps the first experimental evidence that wall deformability can affect the laminar-turbulent transition in tubes with deformable walls. Significant efforts[4,5] over the past two decades have shed light on qualitatively different mechanisms of instabilities that arise due to the flow in this coupled system. Technological devices such as lab-on-a-chip applications and microfluidic devices[6,7] use soft solid elastomeric platforms for fabrication, and it is possible to tune the elastic modulus in such systems to facilitate mixing in channels at small length scales by inducing instabilities in the system.

There are two key non-Newtonian features that can play a role: (i) the viscoelastic nature of the fluid, and (ii) the shear-rate dependence of material properties like the viscosity of the fluid. While in a real polymeric fluid both of these features can become relevant simultaneously, from a theoretical standpoint, it is often instructive to isolate these two effects in order to study their consequences. Such an exercise would help in identifying the consequences of these distinct non-Newtonian effects of the polymer solution on the stability of the flow. While the role of viscoelasticity of the fluid on the stability has been addressed in some previous studies[8–12], the consequences of shear-rate dependent viscosity has not received much attention barring a few studies[13,14]. The aim of the present work is to understand the role of shear-thinning on the stability of the flow past a deformable solid, with the fluid being modeled using both the power law and Carreau models[15,16]. While the power-law model has been used in many studies to analyze the stability of non-Newtonian flows, the model however introduces singularities in the limit of zero shear-rates, which thence renders the model physically unrealistic[17]. The Carreau model overcomes this limitation, and has a well-defined zero-shear viscosity. The study on the combined plane Couette-Poiseuille flow of the Carreau fluid in a rigid channel by Nouar and Frigaard[18] explored the role of the wall velocity and shear thinning behavior on the stability. The work reported that wall velocity has a stabilizing effect on the plane Couette-Poiseuille flow and that increasing the shear-thinning behavior stabilizes the long wavelength modes.

The earlier studies on flow past deformable solid surfaces uncovered modes of instability not present in flow past rigid surfaces. Gkanis and Kumar[19] studied the instability of a creeping Couette flow past a deformable solid modeled as a frame-invariant neo-Hookean model, after initial works used a linear viscoelastic model[20–23] and spring-backed plate model[24] to describe the deformable solid. The neo-Hookean model is nonlinear in the deformation gradient and is valid for finite deformations[25]. Analysis of Hagen-Poiseuille flow in a deformable tube predicted an instability in the creeping-flow limit for the linear elastic model[26], while it did not for the neo-Hookean model[27]. These ambiguities were reconciled recently by Patne *et al.*[28], who presented a consistent formulation for different geometric configurations.

The recent experimental work of Srinivas and Kumaran[29] showed for rectangular channel flows with deformable walls that the addition of polyacrylamide to the flow reduced the critical Re, thus showing that the addition of polymers has a destabilizing effect on the instabilites present in Newtonian flow past soft solid surfaces. The shear rates for the polymer solutions flowing in the microchannels are extremely large. Estimating the velocity of the fluid in the tube to be around 1 m/s and the channel half width to be 500 µm, the typical estimate for the shear rate would be $2000\,\mathrm{s}^{-1}$. At such high shear-rates the shear-thinning behavior could play a very important role in experimental observations involving microscale flows.

The role of the fluid elasticity on the flow past a deformable solid was theoretically explored first by Shankar and Kumar[8] in the creeping-flow limit. The analysis predicted unstable modes beyond a critical strain rate and was successful in recovering not only the stable modes found by Gorodtsov and Leonov[30] for a rigid surface, but also the unstable viscous modes reported by Kumaran *et al.*[31]. A subsequent study[32] continued the unstable mode in the creeping-flow limit to high Re and showed that at $\Gamma \propto Re^{-1/3}$ for the unstable modes in that limit. This scaling is characteristic of a class of modes called 'wall modes' in a Newtonian fluid[33] wherein the perturbations in the fluid are confined near the deformable wall in a thin region of thickness $O(Re^{-1/3})$. The results of Ref. 32 show that the scaling exponent $(-1/3)$ remains unchanged when viscoelastic effects are present in the fluid. Chokshi *et al.*[12] extended the analysis of the stability of elastic fluids due to the addition of dilute polymers past deformable surfaces to high Re. The plane Couette flow of the Oldroyd-B fluid showed a scaling of $\Gamma \sim Re^{-\frac{1}{3}}$ for the wall modes and a scaling of $\Gamma \sim Re^{-1}$ for the inviscid modes.

Although the study of viscoelastic fluids using the Oldroyd-B model provides an insight into the stability of fluids that are not Newtonian in nature, the model assumes a constant shear-rate-independent viscosity. The role of shear-rate dependent viscosity on the stability of fluid flow past deformable solid surfaces was first explored by Roberts and Kumar[13] for creeping Couette flow of a power-law fluid past a neo-Hookean solid. The analysis showed that the role of shear-thickening/thinning nature of the fluid on the stability of the system is dependent on the thickness of the solid. It was also reported that the critical shear-rate Γ_c, decreases with increase in n for thin solids of thickness $H < 3$, and for thicker solids, $H > 3$, Γ_c increases with increase in n, where n is the power-law index. Giribabu and Shankar[14] extended this work for the power-law fluid at finite Reynolds numbers and found that the unstable wall modes scale as $\Gamma \sim Re^{\frac{-1}{2n+1}}$. This dependence on n highlights the role of the non-Newtonian nature of the fluid and it was shown to be consistent with previously established results for the Newtonian case[34]. Pourjafar *et al.*[35] analyzed the creeping plane Poiseuille flow past a Mooney-Rivlin solid to investigate the role played by the power-law index, n, on the critical pressure gradient. The shear-thinning nature of the fluid was stabilizing and the shear-thickening fluid was seen to be destabilizing in comparison to the Newtonian fluid. An extension[36] of this work showed that at a non-zero Reynolds number, the effect of shear-thinning on the flow could be stabilizing or destabilizing depending on the power-law index n and Re.

The problem of fluid flow past a deformable surface involves the coupling of the fluid and wall dynamics. The coupled system can be non-dimensionalized either by using scales from the fluid flow properties (referred here as 'rigid' scaling), or by using scales from the deformable solid (referred here as 'deformable' scaling). The rigid scaling uses a characteristic velocity scale that is imposed by the base flow, while the deformable scaling is material-dependent and uses the shear modulus of the solid to scale the stresses. Although different scalings could reduce to differing governing equations, the solution and characteristics of a given problem should remain similar regardless of the non-dimensionalization scheme. While this is true in most cases, it turns out that for the power-law model that does not have an intrinsic viscosity scale, there is some ambiguity in defining the scales for non-dimensionalization. This aspect is further discussed and clarified in detail in this work.

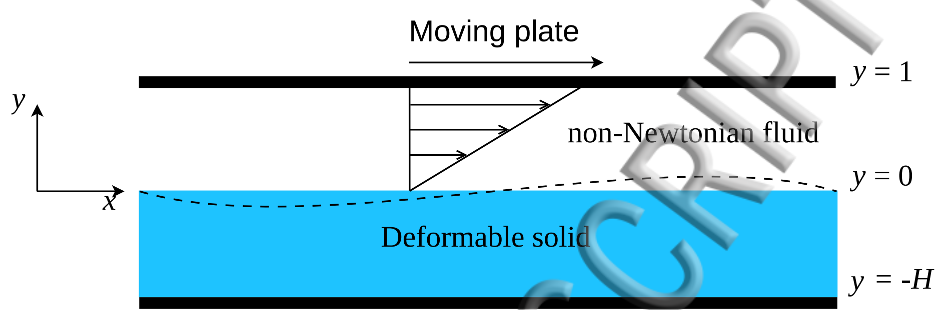

FIG. 1. Schematic representation of plane Couette flow of a non-Newtonian fluid past a deformable solid in the non-dimensional coordinate system.

Previous works[13,14] on the stability of power-law fluid past the deformable solid use a deformable non-dimensionalization scheme to analyze the problem. When we revisited the previous formulations, we identified an algebraic error in both Roberts and Kumar [13] and in Giribabu and Shankar [14], which we now correct in the present study. We show that when the appropriate corrections are made, there are quantitative differences in the stability results. This discrepancy is shown to arise from an incorrect usage of the deviatoric stress tensor in the derivation of the linearised momentum equations for the fluid flow. Upon comparing the formulations of the previous studies that used deformable scalings with the rigid scalings used in this study, we establish some fundamental shortcomings of the power-law fluid model in describing the stability behavior. To address these shortcomings, we use in this study the Carreau model which has a well-defined zero-shear rate viscosity. The advent of experimental studies[29,37,38] to corroborate theoretical predictions reinforces the importance of obtaining results that are unambiguous and are independent of the non-dimensionalization scheme employed. The main objective of this work is to resolve the inconsistency inherently present in the power-law fluid, by carrying out the analysis using the Carreau fluid. We further delineate the role of the shear-rate dependent viscosity on the stability past a deformable solid for a wide range of Re. The earlier study of Chokshi et al.[12] has shown that viscoelastic effects (as modeled using the Oldroyd-B equation) have a destabilizing role on the wall mode instability. However, while the experiments of Srinivas and Kumaran[29] also indicate a destabilizing role, the shear rates prevailing in the experiments are very large (~ 5000 s^{-1}). Thus, it can be expected that the shear thinning nature of the fluid could be relevant to the experimental conditions. The role of fluid shear thinning on the wall mode instability has not been addressed thus far, and this provides another motivation for the present study.

The remainder of this paper is organized as follows: The problem is formulated and the governing equations of the coupled system are presented in Section II for both the rigid and deformable scalings. The results from the linear stability analysis are discussed in Section III. Finally, the salient conclusions are summarized in Section IV.

II. PROBLEM FORMULATION

The schematic of the system under consideration, shown in Fig. 1, is that of Couette flow of an incompressible, non-Newtonian fluid of density, ρ^*, past a deformable solid. The power-law and Carreau models[15,16] are used to describe the flow of the non-Newtonian fluid which occupies the region $0 < y^* < R^*$ where superscript asterisk (*) denotes a dimensional quantity. The deformable solid is modeled as an incompressible, impermeable neo-Hookean solid with shear modulus, G^* and density ρ^*. The neo-Hookean solid is assumed to be purely elastic and dissipative effects are negligible. Although realistic elastomeric meterials would have some dissipative effects, previous studies[39,40] have shown that the effect of dissipation had a negligible effect on the finite-wavenumber instabilities at both low and high Reynolds numbers. Hence, we restrict this study to a purely elastic neo-Hookean solid. The neo-Hookean solid of thickness HR^* is perfectly bonded onto a rigid surface at $y^* = -HR^*$, with H being the dimensionless ratio of solid to fluid thickness. The top rigid plate moves with a dimensional velocity of V_m^*.

The stress tensor for a non-Newtonian fluid in its dimensional form is given by the sum of a pressure contribution and a deviatoric contribution, $\boldsymbol{\tau}^*$, $\boldsymbol{\mathcal{T}^*} = -p_f^*\mathbf{I} + \boldsymbol{\tau}^*$. The deviatoric stress is given by

$$\boldsymbol{\tau}^* = \eta^*(\mathrm{II}^*)\dot{\boldsymbol{\gamma}}^* \tag{1}$$

where $\dot{\boldsymbol{\gamma}}^{\boldsymbol{*}} = \nabla \boldsymbol{v}^* + (\nabla \boldsymbol{v}^*)^T$ is the rate-of-strain tensor. Here $\boldsymbol{v^*} = (v_x^*, v_y^*, v_z^*)$ is the velocity field with v_i^* representing the dimensional velocity component in the i-direction. The second invariant of the rate-of-strain tensor, II^*, is given by

$$\mathrm{II}^*_{\dot{\gamma}^*} = \sqrt{\frac{1}{2}(\dot{\gamma}^*{}_{ij}\dot{\gamma}^*{}_{ji})},$$

where $i, j = 1, 2, 3$ denoting the three Cartesian directions. The dependence of the viscosity term on the shear-rate reflects the non-Newtonian nature of the fluid. The simple power-law model is given by[17]

$$\eta^* = m^*\mathrm{II}^{*(n-1)}_{\dot{\gamma}^*}, \tag{2}$$

where n is the power-law index and m^* is the consistency index, which has fractional dimensions because of the non-integral values n can take. In order to render m^* appear like a viscosity, following Roberts and Kumar[13], we express $m^* = \hat{m}^*\eta_f^*$, where η_f^* has the dimensions of viscosity. The arbitrariness arises in the specification of $\hat{m}^*$ in the different schemes of non-dimensionalization. Previous works by Roberts and Kumar[13] as well as Giribabu and Shankar[14] use a non-dimensional scheme (henceforth referred to as 'deformable scaling') to non-dimensionalize the governing equations and constitutive relations. This work explores the consequences of both rigid and deformable scalings, the consequences of which are presented in the next section. The shear-dependent viscosity for the Carreau model[15] is given by,

$$\eta^* = \eta^*_\infty + (\eta^*_0 - \eta^*_\infty)(1 + (\lambda^*\mathrm{II}^*_{\dot{\gamma}^*})^2)^{\frac{n-1}{2}}, \tag{3}$$

where λ^* is the time constant, n is a power-law like index, η_0^* represents the zero-shear viscosity and η^*_∞ represents the infinite-shear viscosity. In the above equation, when the exponent 2 in the γ^{*2} term and the denominator of the exponent $(n-1)/2$ are different from 2, then the model is referred to as the Carreau-Yasuda model[17]. It can be seen that η_0^* can be used as an unambiguous viscosity scale in this model to non-dimensionalize the constitutive relation. Fig. 2 shows the variation of the viscosity in the base state for the Carreau fluid with the second invariant of the rate of strain tensor. At low strain rates, the viscosity of the fluid is the zero-shear viscosity, η_0^*, and the fluid is Newtonian in nature. Similarly, at high strain rates, the viscosity of the fluid is the infinite-shear viscosity, η_∞^*, and the fluid is Newtonian in nature.

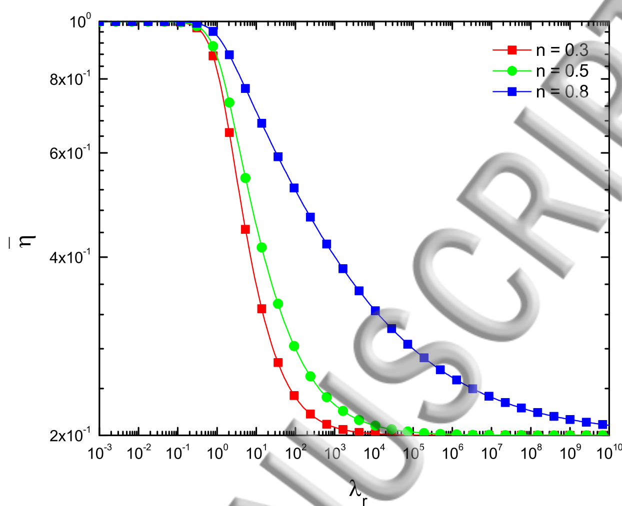

FIG. 2. Variation of the viscosity at the base state, $\bar{\eta} \equiv \eta^*/\eta_0^*$ for the Carreau fluid with the non-dimensional shear rate $\lambda_r \equiv \lambda_r^* R^*/V_m^*$ for $\eta_\infty^*/\eta_0^* = 0.2$ and different values of n.

We model the solid as a neo-Hookean solid using a Lagrangian three-state (L3) formulation described by Patne *et al.*[41]. The neo-Hookean model is considered due to its validity even at finite deformations. The three states of deformation that are considered in the derivation are the undeformed, pre-stressed and the perturbed states. The flow of the fluid past the initially undeformed solid imposes a stress field on the solid. We represent the reference position vector of a particle on the initially undeformed solid, at $t^* = 0$ by $\mathbf{X}^* = (X_1^*, X_2^*, X_3^*)$. The position vector of the particle is given by

$$\bar{\mathbf{x}}^*(\mathbf{X}^*) = \mathbf{X}^* + \bar{u}^*(\mathbf{X}^*), \tag{4}$$

where $\bar{\mathbf{x}}^* = (\bar{x}_1^*, \bar{x}_2^*, \bar{x}_3^*)$ is the position of the particle at any time t^*, and $\bar{u}^*$ is the displacement vector of the particle arising due to the fluid motion. The incompressibility condition of the neo-Hookean solid at the base state gives

$$\det(\bar{\mathbf{F}}^*) = 1, \tag{5}$$

where $\bar{\mathbf{F}}^* = \frac{\partial \bar{\mathbf{x}}^*}{\partial \mathbf{X}^*}$ is the base state deformation gradient. The Cauchy stress tensor of the solid in dimensional form is,

$$\boldsymbol{\sigma}^* = -p_g^* \mathbf{I} + G^*(\mathbf{F}^* \cdot \mathbf{F}^{*\mathbf{T}}), \tag{6}$$

where G^* is the shear modulus of the neo-Hookean solid. The conservation of momentum in the neo-Hookean solid is represented by

$$\rho_g^* \frac{\partial^2 \boldsymbol{u}^*}{\partial t^{*2}} = \nabla_{\mathbf{X}^*} \cdot \mathbf{P}^*, \tag{7}$$

where ρ_g^* is the density of the solid and $\mathbf{P}^*$ is the first Piola-Kirchoff stress tensor, which is defined as

$$\mathbf{P}^* = \mathbf{F}^{*-1} \cdot \boldsymbol{\sigma}^*. \tag{8}$$

A. Rigid Scaling

While using the rigid scaling, the length scale is non-dimensionalized by R^*, while the time scale is non-dimensionalized by R^*/V_m^*. The continuity equation, which is independent of the manner in which it is scaled, is given by

$$\nabla \cdot \boldsymbol{v} = 0. \tag{9}$$

The non-dimensional momentum equation for fluid flow using the rigid scaling is given by

$$Re\frac{D\boldsymbol{v}}{Dt} = -\nabla p_f + \nabla \cdot \boldsymbol{\tau}, \tag{10}$$

The constitutive relation for the power-law fluid is given by

$$\eta = \mathrm{II}_{\dot{\gamma}}^{(n-1)}, \tag{11}$$

where the viscosity, η is scaled by $\eta_f^* \equiv \frac{m^*}{\hat{m}^*}$ and $m^r = \hat{m}^*\left(\frac{V_m^*}{R^*}\right)^{n-1}$ is set to 1. The superscripts r for the consistency index used in Eq. (11) denote the ('rigid') scaling used to non-dimensionalize the equations. The dimensionless variable m^r can be set to any numerical value based on the consistency index of the fluid. Setting m^r to unity implies a particular choice for the (dimensional) consistency index of the fluid. For the Carreau model, the constitutive relation is

$$\eta = \eta_\infty + (1-\eta_\infty)(1+(\lambda_r \mathrm{II}_{\dot{\gamma}})^2)^{\frac{n-1}{2}}, \tag{12}$$

where η_0^* is used to scale viscosity and $\lambda_r = \lambda_r^* R^*/V_m^*$. It must be noted that the dimensionless parameter λ_r is a flow-dependent quantity, and represents the dimensionless shear rate of the base flow. Thus if λ_r is fixed, then the shear rate dependence of the viscosity is no longer present. It is possible to rewrite this in terms of a flow-independent quantity as $\lambda_r = \tilde{\lambda}_r Re$ where $\tilde{\lambda}_r \equiv \lambda^* \eta_0^*/(\rho R^{*2})$ is the flow-independent quantity that denotes the onset of shear thinning. With this, the above equation becomes

$$\eta = \eta_\infty + (1-\eta_\infty)(1+(\tilde{\lambda}_r Re \mathrm{II}_{\dot{\gamma}})^2)^{\frac{n-1}{2}}. \tag{13}$$

In the base state, the dimensionless second invariant (in rigid scalings) becomes $\mathrm{II}_{\dot{\gamma}} = 1$ and so the viscosity function (in base state only) in rigid scaling is given by

$$\eta = \eta_\infty + (1-\eta_\infty)(1+(\tilde{\lambda}_r Re)^2)^{\frac{n-1}{2}}. \tag{14}$$

By fixing $\tilde{\lambda}_r$ constant, the viscosity in the above equation undergoes shear thinning as Re is increased, unlike Eq. 12 which does not exhibit shear thinning if λ_r is kept constant. When we discuss the results in Section III, we explore the consequences of keeping both λ_r and $\tilde{\lambda}_r$ constant.

The stresses (including pressure) are non-dimensionalized by $\frac{\eta_f^{*r} V_m^*}{R^*}$ for the power-law fluid and by $\frac{\eta_0^* V_m^*}{R^*}$ for the Carreau fluid. Non-dimensionalizing the governing equations for the solid, we obtain the non-dimensionalized Cauchy stress tensor,

$$\boldsymbol{\sigma} = -p_g \mathbf{I} + \frac{1}{\Gamma_r}(\mathbf{F} \cdot \mathbf{F^T}), \tag{15}$$

where Γ_r is defined as the non-dimensional strain rate, given by $\frac{\eta_f^{*r} V_m^*}{G^* R^*}$ for the power-law fluid and by $\frac{\eta_0^* V_m^*}{G^* R^*}$ for the Carreau fluid. The momentum conservation equation for the neo-Hookean solid thus becomes,

$$Re \frac{\partial^2 \boldsymbol{u}}{\partial t^2} = \nabla_{\mathbf{X}} \cdot \mathbf{P}, \tag{16}$$

In the base state, we assume that the fluid and solid are at steady state. The interface is flat and undeformed, at $y = 0$. For the plane Couette flow, the base state velocity profile is given by the linear velocity distribution $\bar{\boldsymbol{v}} = (y, 0, 0)$ for the following reason. The linear velocity profile implies a constant shear rate across the flow, and therefore the viscosity remains a constant in the flow domain. This thus implies that the linear velocity profile for plane Couette flow of a Newtonian fluid remains a solution to the Carreau model as well. However, for pressure-driven flows in a channel with varying shear-rates in the wall-normal direction, the Newtonian velocity profile is no longer valid for shear-thinning fluids. The base state deformation for the solid is obtained by solving Eq. (16), which is the non-dimensionalized momentum balance equation, at the base state while factoring in the tangential stress balance at the interface and no-slip conditions at the rigid wall. The first Piola-Kirchoff stress tensor in the base state is related to the Cauchy stress tensor as

$$\bar{\mathbf{P}} = \bar{\mathbf{F}}^{-1} \cdot \bar{\boldsymbol{\sigma}}, \tag{17}$$

$$\nabla_{\bar{\mathbf{x}}} \cdot \bar{\mathbf{P}} = 0. \tag{18}$$

The base state for the deformation of the solid for power-law and Carreau fluid are

$$\bar{u}_1 = \Gamma_r (X_2 + H) \quad \text{Power-law fluid,} \tag{19}$$

$$\bar{u}_1 = \Gamma_r (\eta_\infty + (1 - \eta_\infty)(1 + \tilde{\lambda}_r^2 Re^2)^{\frac{n-1}{2}})(X_2 + H) \quad \text{Carreau fluid.} \tag{20}$$

It can thus generally be expressed as

$$\bar{u}_1 = \Gamma_r t_1^r (X_2 + H), \tag{21}$$

Here, t_1^r is specific to the non-Newtonian model used for the fluid. The superscript, r, denotes the rigid scaling to make a distinction from the deformable scaling.

$$t_1^r = 1 \quad \text{Power-law fluid,} \tag{22}$$

$$t_1^r = \eta_\infty + (1 - \eta_\infty)\big(1 + \tilde{\lambda}_r^2 Re^2\big)^{\frac{n-1}{2}} \quad \text{Carreau fluid.} \tag{23}$$

We impose two-dimensional, infinitesimal perturbations which have normal modes of the form

$$f'(x, y, t) = \tilde{f}(y) e^{ik(x - ct)}, \tag{24}$$

where f' represents perturbation to any dynamical quantity in the fluid and solid. Here, k is the wavenumber, c is the complex wave speed, which can be expressed as $c = c_r + ic_i$. The system is temporally unstable when the imaginary part of the complex wave speed, $c_i > 0$, indicating that the disturbances grow in time. The linearised perturbation equations for the rigid scaling are,

$$ik\tilde{v}_x + \mathrm{D}\tilde{v}_y = 0, \tag{25}$$

$$Re\big(ik(y-c)\tilde{v}_x + \tilde{v}_y\big) = -ik\tilde{p}_f - t_1^r(2k^2\tilde{v}_x) + t_2^r(\mathrm{D}^2\tilde{v}_x + ik\mathrm{D}\tilde{v}_y), \tag{26}$$

$$Re\big(ik(y-c)\tilde{v}_y\big) = -\mathrm{D}\tilde{p}_f + t_2^r(ik\mathrm{D}\tilde{v}_x - k^2\tilde{v}_y) + t_1^r(2\mathrm{D}^2\tilde{v}_y), \tag{27}$$

where t_2^r is given by

$$t_2^r = n \quad \text{Power-law} \tag{28}$$

$$t_2^r = \eta_\infty + \left[1 + \frac{\tilde{\lambda}_r^2 Re^2}{1+\tilde{\lambda}_r^2 Re^2}(n-1)\right](1-\eta_\infty)\big(1+\tilde{\lambda}_r^2 Re^2\big)^{\frac{n-1}{2}} \quad \text{Carreau} \tag{29}$$

For the solid, we perturb the current position vector of the pre-stressed representative material points by means of applying infinitesimal perturbations as follows:

$$\mathbf{x}(\bar{\mathbf{x}}) = \bar{\mathbf{x}} + \mathbf{u}'(\bar{\mathbf{x}}, t). \tag{30}$$

The deformation gradient $\mathbf{F}$ highlights a relationship between the undeformed state and the perturbed state. In order to obtain a relationship between the overall deformation gradient and the deformation gradients related to the pre-stressed state, the following manipulation is made[42],

$$\mathbf{F} = \frac{\partial \mathbf{x}}{\partial \mathbf{X}} = \frac{\partial \mathbf{x}}{\partial \bar{\mathbf{x}}} \cdot \frac{\partial \bar{\mathbf{x}}}{\partial \mathbf{X}} = \mathbf{F}' \cdot \bar{\mathbf{F}}, \tag{31}$$

here $\mathbf{F}'$ denotes the perturbed state deformation gradient. The incompressibility condition for the perturbed state becomes $\det(\mathbf{F}') = 1$. The first Piola-Kirchoff stress defined with respect to the pre-stressed state as the reference is given by

$$\mathbf{P} = \mathbf{F}'^{-1} \cdot \boldsymbol{\sigma}. \tag{32}$$

The momentum balance equation, after perturbing the solid, is given as

$$Re\frac{\partial^2 \boldsymbol{u}}{\partial t^2} = \nabla_{\bar{\mathbf{x}}} \cdot \mathbf{P}. \tag{33}$$

The linearised equations for the solid using the L3 formulation are,

$$ik\tilde{u}_1 + \mathrm{D}\tilde{u}_2 = 0, \tag{34}$$

$$-ik\tilde{p}_g + \frac{1}{\Gamma_r}(D^2 - k^2)\tilde{u}_1 - k^2\Gamma_r t_1^{2r}\tilde{u}_1 + 2t_1^r ik\mathrm{D}\tilde{u}_1 = -k^2c^2Re\tilde{u}_1, \tag{35}$$

$$-\mathrm{D}\tilde{p}_g + \frac{1}{\Gamma_r}(D^2 - k^2)\tilde{u}_2 - k^2\Gamma_r t_1^{2r}\tilde{u}_2 + 2t_1^r ik\mathrm{D}\tilde{u}_2 = -k^2c^2Re\tilde{u}_2, \tag{36}$$

where $\mathrm{D} = \frac{d}{d\bar{x}_2}$. The linearised interface conditions are

$$\tilde{v}_y + ikc\tilde{u}_2 = 0, \tag{37}$$
$$ikc\tilde{u}_1 + \tilde{v}_x + \tilde{u}_2 = 0, \tag{38}$$
$$\frac{1}{\Gamma_r}\big(\mathrm{D}\tilde{u}_1 + ik\tilde{u}_2\big) = t_2^r\big(\mathrm{D}\tilde{v}_x + ik\tilde{v}_y\big), \tag{39}$$
$$-\tilde{p}_g + \frac{2}{\Gamma_r}\mathrm{D}\tilde{u}_2 + 2ikt_1^r\tilde{u}_2 + \frac{k^2 T}{\Gamma_r}\tilde{u}_2 = -\tilde{p}_f + 2t_1^r\mathrm{D}\tilde{v}_y, \tag{40}$$

where T denotes the surface tension at the interface. The boundary conditions at $y = 1$ and $y = 1 + H$ are

$$\tilde{v}_x = 0, \quad \tilde{v}_y = 0 \quad \text{at } y = 1, \tag{41}$$
$$\tilde{u}_1 = 0, \quad \tilde{u}_2 = 0 \quad \text{at } y = -H. \tag{42}$$

B. Deformable Scaling

While using the deformable scaling, the length scale is non-dimensionalized by R^* and stresses (including pressure) by G^*. The non-dimensionalized governing equation for the fluid flow using the deformable scaling is given by,

$$\frac{Re}{\Gamma_d}\frac{D\boldsymbol{v}}{Dt} = -\nabla p_f + \nabla \cdot \boldsymbol{\tau}, \tag{43}$$

The non-dimensional strain-rate, Γ_d, is given by $\frac{\eta_f^d V_m^*}{G^* R^*}$ for the power-law fluid and by $\frac{\eta_0^* V_m^*}{G^* R^*}$ for the Carreau fluid. It is worth mentioning that for the Carreau fluid, Γ remains the same for both rigid and deformable scalings, and hence Γ will be presented without the subscript (d or r) for the Carreau fluid. The simple power-law model is non-dimensionalized to obtain the constitutive relation,

$$\eta = \mathrm{II}_{\dot{\gamma}}^{(n-1)}, \tag{44}$$

where the viscosity, η, is scaled by $\eta_f^* \equiv \frac{m^*}{\hat{m}^*}$ and $m^d = \hat{m}^* \left(\frac{G^*}{\eta_f^*}\right)^{n-1}$ is set to 1. It is worth mentioning here that different (non-dimensional) quantities are being set to unity in both rigid and deformable scalings, which is the origin of the difference between the two results. For the Carreau fluid, the non-dimensionalized form becomes,

$$\eta = \eta_\infty + (1 - \eta_\infty)(1 + (\lambda_d \mathrm{II}_{\dot{\gamma}})^2)^{\frac{n-1}{2}}, \tag{45}$$

where η_0^* is used to scale viscosity and η_0^*/G^* is used to scale λ_d. It must be noted that λ_d is independent of the flow velocity V_m^*, and can be written in terms of $\tilde{\lambda}_r$ as $\lambda_d = \tilde{\lambda}_r Re/\Gamma$. Thus, fixing λ_d constant and $\tilde{\lambda}_r$ constant are not equivalent, though both are flow-independent dimensionless quantities. In the base state (under deformable scalings), the second invariant $\mathrm{II}_{\dot{\gamma}} = \Gamma$ and hence the above viscosity function becomes (in the base state only)

$$\eta = \eta_\infty + (1 - \eta_\infty)(1 + (\tilde{\lambda}_r Re)^2)^{\frac{n-1}{2}}, \tag{46}$$

When the above equation is compared with Eq. 14, we note that both the equations are identical if $\tilde{\lambda}_r$ is kept constant. The time scale is non-dimensionalized by η_f^*/G^* for the power-law fluid and is scaled by η_0^*/G^* for the Carreau fluid. Having established the scalings, it is easy to match the results between the rigid and deformable scalings for the respective non-Newtonian viscosity models by replacing non-dimensional scheme appropriately.

The base state velocity profile while using the deformable scaling is $\bar{\boldsymbol{v}} = (\Gamma_d y, 0, 0)$. We proceed to evaluate the base state deformation of the solid for the deformable scaling. The non-dimensional Cauchy stress tensor obtained is of the form,

$$\boldsymbol{\sigma} = -p_g \mathbf{I} + (\mathbf{F} \cdot \mathbf{F^T}). \tag{47}$$

The momentum balance equation for the neo-Hookean solid using the deformable scaling is,

$$\frac{Re}{\Gamma_d}\frac{\partial^2 \boldsymbol{u}}{\partial t^2} = \nabla_{\bar{\mathbf{x}}} \cdot \mathbf{P}. \tag{48}$$

Solving the non-dimensionalized momentum balance equation for the base state, we obtain the deformation of the solid

$$\bar{u}_1 = \Gamma_d t_1^d (X_2 + H) \tag{49}$$

The variables t_1^d and t_2^d for the deformable scaling are presented below. For the Carreau fluid,

$$t_1^d = \eta_\infty + (1-\eta_\infty)\big(1+\lambda_d^2\Gamma_d^2\big)^{\frac{n-1}{2}}$$
$$t_2^d = \eta_\infty + \left[1 + \frac{\lambda_d^2\Gamma_d^2}{1+\lambda_d^2\Gamma_d^2}(n-1)\right](1-\eta_\infty)\big(1+\lambda_d^2\Gamma_d^2\big)^{\frac{n-1}{2}}$$

For the power-law fluid,

$$t_1^d = \Gamma_d^{n-1},$$
$$t_2^d = n\Gamma_d^{n-1}.$$

The base state deformations for the power-law and Carreau fluids are

$$\bar{u}_1 = \Gamma_d^n (X_2 + H) \quad \text{Power-law fluid} \tag{50}$$
$$\bar{u}_1 = \Gamma_d(\eta_\infty + (1-\eta_\infty)(1+\lambda_d^2\Gamma_d^2)^{\frac{n-1}{2}})(X_2 + H) \quad \text{Carreau fluid} \tag{51}$$

A key reason for the difference between Eqs. (19) and (50) for the power-law fluid and Eqs. (20) and (51) for the Carreau fluid stem from the base state velocity profile of the fluid region in both the scalings, with $\bar{v}_x$ being equal to y for the rigid scaling and $\Gamma_d y$ for the deformable scaling. Imposing two-dimensional, infinitesimal perturbations and using the method of normal modes defined in Eq. (24), we linearise the governing equations for the system. The linearised governing equations are

$$ik\tilde{v}_x + \mathrm{D}\tilde{v}_y = 0, \tag{52}$$
$$\frac{Re}{\Gamma_d}\big(ik(\Gamma_d y - c)\tilde{v}_x + \Gamma_d \tilde{v}_y\big) = -ik\tilde{p}_f - t_1^d(2k^2\tilde{v}_x) + t_2^d(\mathrm{D}^2\tilde{v}_x + ik\mathrm{D}\tilde{v}_y), \tag{53}$$
$$\frac{Re}{\Gamma_d}\big(ik(\Gamma_d y - c)\tilde{v}_y\big) = -\mathrm{D}\tilde{p}_f + t_2^d(ik\mathrm{D}\tilde{v}_x - k^2\tilde{v}_y) + t_1^d(2\mathrm{D}^2\tilde{v}_y). \tag{54}$$

The linearised governing equations for the solid are

$$ik\tilde{u}_1 + \mathrm{D}\tilde{u}_2 = 0, \tag{55}$$

$$-ik\tilde{p}_g + (\mathrm{D}^2 - k^2)\tilde{u}_1 - k^2\Gamma_d^2 t_1^{2d}\tilde{u}_1 + 2\Gamma_d t_1^d ik\mathrm{D}\tilde{u}_1 = -\frac{Re}{\Gamma_d}k^2c^2\tilde{u}_1, \tag{56}$$

$$-\mathrm{D}\tilde{p}_g + (\mathrm{D}^2 - k^2)\tilde{u}_2 - k^2\Gamma_d^2 t_1^{2d}\tilde{u}_2 + 2\Gamma_d t_1^d ik\mathrm{D}\tilde{u}_2 = -\frac{Re}{\Gamma_d}k^2c^2\tilde{u}_2, \tag{57}$$

$$\tag{58}$$

where $\mathrm{D} = \frac{d}{d\bar{x}_2}$. The linearised boundary conditions are

$$\tilde{v}_y + ikc\tilde{u}_2 = 0, \tag{59}$$

$$ikc\tilde{u}_1 + \tilde{v}_x + \Gamma_d\tilde{u}_2 = 0, \tag{60}$$

$$\mathrm{D}\tilde{u}_1 + ik\tilde{u}_2 = t_2^d(\mathrm{D}\tilde{v}_x + ik\tilde{v}_y), \tag{61}$$

$$-\tilde{p}_g + 2\mathrm{D}\tilde{u}_2 + 2ik\Gamma_d t_1^d\tilde{u}_2 + k^2\Gamma\tilde{u}_2 = -\tilde{p}_f + 2t_1^d\mathrm{D}\tilde{v}_y. \tag{62}$$

The boundary conditions at $y = 1$ and $y = 1 + H$ are

$$\tilde{v}_x = 0, \quad \tilde{v}_y = 0 \quad \text{at } y = 1, \tag{63}$$

$$\tilde{u}_1 = 0, \quad \tilde{u}_2 = 0 \quad \text{at } y = -H. \tag{64}$$

This deformable formulation corrects the algebraic error in the formulation of the linearised governing equations of the power-law fluid past a neo-Hookean deformable solid in previous works[13,14]. In order to resolve Eq. (43) into its x and y-components, the divergence of the stress tensor is represented as,

$$\nabla\cdot\boldsymbol{\tau} = \left(\frac{\partial}{\partial x}\tau_{xx} + \frac{\partial}{\partial y}\tau_{yx}\right)\hat{\mathbf{e}}_x + \left(\frac{\partial}{\partial x}\tau_{xy} + \frac{\partial}{\partial y}\tau_{yy}\right)\hat{\mathbf{e}}_y,$$

where $\hat{\mathbf{e}}_x$ and $\hat{\mathbf{e}}_y$ are unit vectors in the x and y directions. While deriving the x and y-momentum equations, Roberts and Kumar[13] and Giribabu and Shankar[14] erroneously considered the elements of both $\hat{\mathbf{e}}_x$ and $\hat{\mathbf{e}}_y$ directions for the respective momentum equations. The extra, erroneous terms vanish for the Newtonian case of $n = 1$ because they are multiplied by a factor of $n - 1$ in the linearised momentum equations of Roberts and Kumar[13] and Giribabu and Shankar[14]. When considering the flow past a deformable solid, the normal stress balance at the interface requires pressure in the fluid at the interface, which when evaluted from the (erroneous) x-momentum equation, gives rise to incorrect results for the eigenvalue c. This discrepancy therefore does not allow for an accurate understanding of the stability of the system. The fourth-order differential equation for the fluid derived by Roberts and Kumar[13] remains the same however, despite the algebraic errors in the linearised momentum equations, because the erroneous terms cancel out due to a manifestation of the continuity equation while eliminating the pressure term. Thus, Giribabu and Shankar[14] were able to produce exact matches of the eigenvalue spectrum with that of Liu and Liu[43] because for the special case of a rigid channel, the fourth order differential equation used to obtain the results was correct.

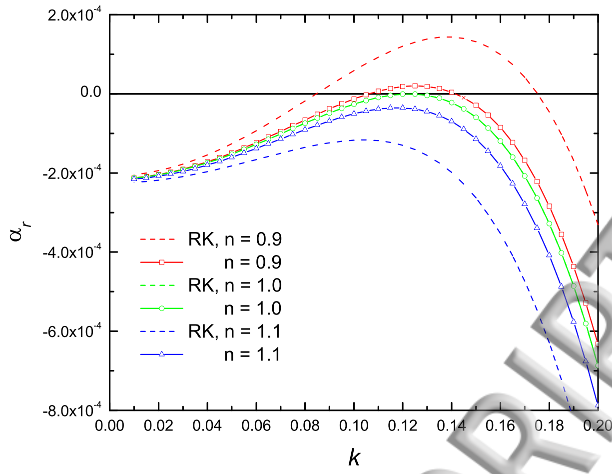

FIG. 3. Results from the earlier formulation of Roberts and Kumar [13] (denoted by RK) and the corrected formulation of the present work are plotted to show the difference in the predictions for the power-law fluid. The real part of the growth rate, α_r vs. the wavenumber, k is shown for $Re = 0$, $T = 10$, $\Gamma_d = 0.34245$, $H = 10$, for different values of the power-law index.

The stability of the system is governed by the Reynolds number, Re, the power-law index, n, the non-dimensionalized infinite-shear viscosity, η_∞, the non-dimensional shear-rate, Γ, the thickness ratio, H and λ. The linearised differential equations for the fluid-solid system along with the boundary conditions of the geometry allow the determination of the stability of the system and form an eigenvalue problem of the form $c^2\mathbf{A}\mathbf{x} + c\mathbf{B}\mathbf{x} + \mathbf{C}\mathbf{x} = 0$, where the matrix $\mathbf{x}$ contains the eigenvectors of the system and $\mathbf{A}, \mathbf{B}, \mathbf{C}$ represent the respective coefficient matrices. The eigenvalue problem is solved for c, which is the wave speed of the system as a function of k, Re, Γ, H, n, λ, η_∞ using a pseudo-spectral collocation method[44]. The veracity of the eigenvalues is checked using a numerical shooting procedure with ortho-normalization[45]. This allows us to numerically evaluate the eigenvalues and stability boundaries. We obtain the eigenspectra using the spectral methods for different values of N (the number of Chebyshev polynomials used to expand the unknown dynamical variables), and choose the value of N for which there is convergence of eigenvalues with N. The shooting code uses an adaptive Runge-Kutta integrator to numerically integrate the differntial equations coupled with a Newton-Raphson interator for the solution of the eigenvalue. The agreement for eigenvalues between the spectral and shooting methods is typically upto six to eight decimal places.

III. RESULTS

In this section, we present the results from the linear stability analysis of the non-Newtonian flow past a neo-Hookean solid. Before analysing the flow modeled by the Carreau fluid, we first present the consequences of correcting the algebraic error made in the previous studies[13,14], by comparing them with the corrected results obtained in the present study for the deformable scaling.

Fig. 3 compares the variation of growth rate, $\alpha = -ikc$, of the most unstable (or least stable) eigenvalue with respect to k for different values of the power-law index, n, for the inaccurate formulation of Roberts and Kumar [13] (denoted by RK) and Giribabu and Shankar [14]

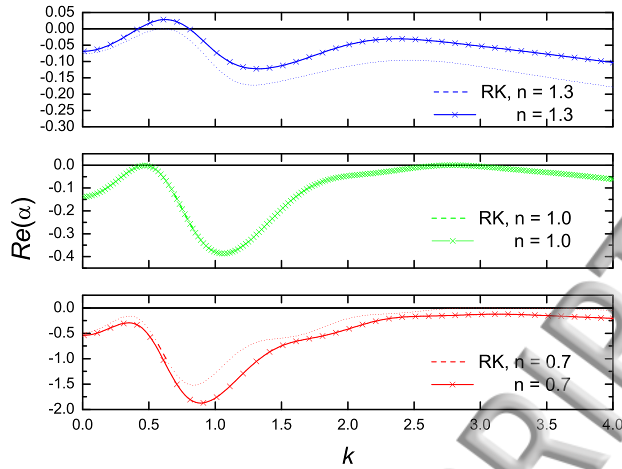

FIG. 4. Comparison of the real part of the growth rate, $Re(\alpha)$ vs. the wavenumber, k, in the creeping-flow limit for $T = 10$, $H = 0.7079$, for different values of the power-law index. For the top plot, $\Gamma_d = 4.258$, the middle plot, $\Gamma_d = 8.669$ and for the bottom plot, $\Gamma_d = 28.67$.

Parameters	k	Giribabu and Shankar	Present work
$n = 1.0, \Gamma_d = 1.0$	0.5	0.36337 + 0.04399i	0.36337 + 0.04399i
$n = 1.0, \Gamma_d = 0.5$	0.5	0.21070 - 0.00235i	0.21070 - 0.00235i
$n = 0.7, \Gamma_d = 0.6$	0.2	0.27181 + 0.02608i	0.27435 + 0.01856i
$n = 1.2, \Gamma_d = 0.8$	0.9	0.25873 - 0.04278i	0.24483 - 0.02320i

Table 1. Complex wave speed (c) obtained (in the creeping-flow limit) from the formulations of Giribabu and Shankar[14] and the corrected formulation of this work in the creeping-flow limit for $H = 10$. Data shows agreement only for $n = 1$.

and the corrected deformable scaling introduced in the present study. The real component of the complex-valued growth rate is given by $\alpha_r = kc_i$. The non-dimensional shear-rate, Γ_d, is chosen such that the system is neutrally stable for the Newtonian case. For $H = 10$, we see that shear thinning has a destabilizing effect, and that shear-thickening fluids are stabilizing. It is seen that as the thickness of the solid with respect to the fluid decreases, this phenomenon is reversed, with the shear-thickening fluids being destabilizing and the shear-thinning fluids being stabilizing in nature.

In an effort to examine the role of solid thickness on the stability of the shear-thickening or shear-thinning fluids, the results of the corrected deformable formulation are compared with that of Roberts and Kumar[13] in Fig. 4. The second sub-plot of the figure shows an exact match for the Newtonian case. This is because the extra, erroneous terms of the previous work become identically zero when $n = 1$. We find that the results of the present study differ only quantitatively with the earlier results, but qualitatively the trends are similar. This assertion is exemplified in Table 1, which compares the eigenvalues for the given set of parameters, while keeping $H = 10$ and $T = 0$. The eigenvalues agree only for the case where $n = 1$. Fig. 5 explores the variation of Γ as a function of k for both the rigid and deformable scalings, the minimum of which gives the critical strain rate, Γ_c for the corresponding k_c. From the results, it is necessary to note the difference in trend of the shear-thickening and shear-thinning fluids. While the trend is consistent for the rigid scaling, the deformable scaling shows that the trend is dependent on the wavenumber k.

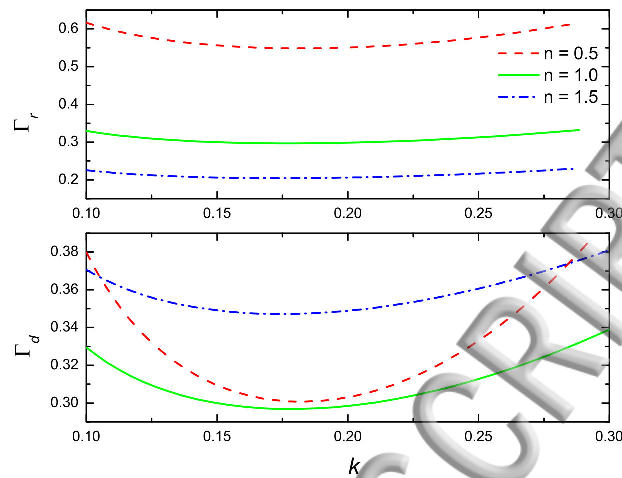

FIG. 5. Comparison of the neutral stability curves in the creeping-flow limit for the power-law fluid at $H = 10$. The top plot presents results from rigid scaling, while the bottom plot shows results from deformable scaling.

We next proceed to examine the effet of shear thinning on the wall mode instabilities at moderate to high Reynolds number. Tracking the finite-wave mode for various values of n to high Re, we observe that the scaling of $\Gamma_d \sim Re^{\frac{-1}{2n+1}}$ for $Re \gg 1$ is obtained for the deformable scaling of the power-law fluid and is in agreement with Giribabu and Shankar [14]. Fig. 6 shows the scaling for the different values of n for the deformable scaling for power-law fluid. The similarity in the slopes is represented in Table 2.

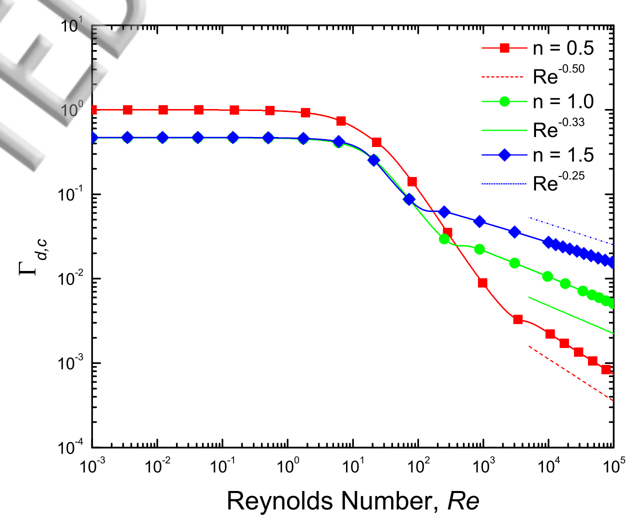

FIG. 6. Variation of the critical strain-rate $\Gamma_{d,c}$ with Re for $k = 0.45$, $H = 10$ and different values of n using the deformable scaling for the power-law fluid. The slope of the curve at high Re varies with n.

Power-law index, n	β from numerics	β (Theoretical)
$n = 0.5$	-0.488	-0.50
$n = 1.0$	-0.318	-0.33
$n = 1.5$	-0.238	-0.25

Table 2. The exponent β in the scaling relation $\Gamma_d \propto Re^{\beta}$ for different values of the power-law consistency index, n.

Interestingly, however, we observe that a similar analysis for the rigid non-dimensionalization scheme shows a scaling of $\Gamma_r \sim Re^{-1/3}$, regardless of the power-law index n as shown in Fig. 7. Physically, this would mean that the scaling for wall mode instability is independent of the shear-thinning/thickening effect of the fluid at an arbitrary Re. The curve as a whole displaces upward with decreasing n, showing the stabilizing effect of the shear-thinning. While the deformable scaling is in agreement with Giribabu and Shankar [14], the rigid scaling shows that irrespective of the power-law index n, the wall modes scale similarly to that of a Newtonian fluid[23,46]. This can be attributed to the way the viscosity is scaled and the terms that are set to unity in the deformable scaling. A relation between Reynolds number using the deformable scaling and rigid scaling is given by

$$Re_d = \left(\frac{\eta_f^*}{G^*}\right)^{n-1} \left(\frac{V_m^*}{R^*}\right)^{n-1} Re_r,$$

$$Re_r = \Gamma_d^{1-n} Re_d,$$

and the non-dimensional strain rate Γ using the deformable scaling and rigid scaling is related by

$$\Gamma_r = \Gamma_d^n.$$

Using the scaling obtained for the rigid non-dimensionalization scheme from Fig. 7, $\Gamma_r \sim Re_r^{-\frac{1}{3}}$, we substitute the relations established to obtain the scaling for the deformable non-dimensionalization scheme seen in Fig. 6.

$$\Gamma_d^n \sim \Gamma_d^{\frac{n-1}{3}} Re_d^{-\frac{1}{3}},$$

$$\Gamma_d \sim Re_d^{\frac{-1}{2n+1}}.$$

We thus show that the dependence of the $\Gamma - Re$ scaling on the power-law index n is purely a consequence of the deformable scaling, since it is not seen in rigid scaling.

However, the question still remains whether the wall mode instability is dependent on the strength of shear thinning, i.e. the power-law index n. This discrepancy of different scalings being observed is due to the ambiguous viscosity scaling for the power-law fluid. The term, η_f, introduced in Section II, merely has dimensions of viscosity, and bears no physical significance. The inability to predict the viscosity at extremely low and high shear-rates also adds to the shortcomings of the power-law model. This warrants the need to explore the Carreau fluid to better capture the physics of the non-Newtonian flow past a deformable solid.

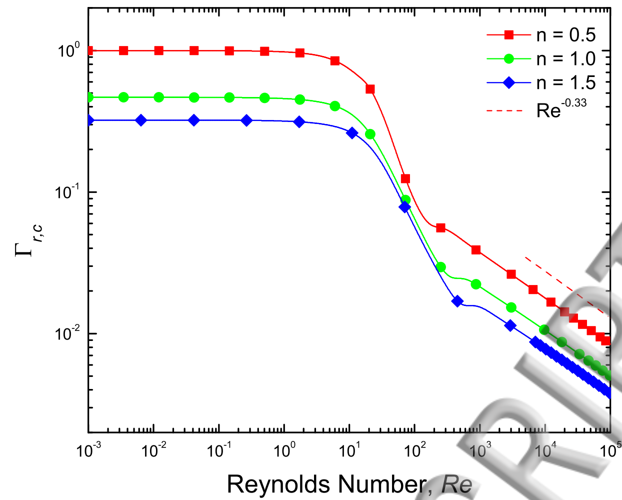

FIG. 7. Variation of the critical strain-rate $\Gamma_{r,c}$ with Re for $k = 0.45$, $H = 10$ and different values of n using the rigid scaling for the power-law fluid.

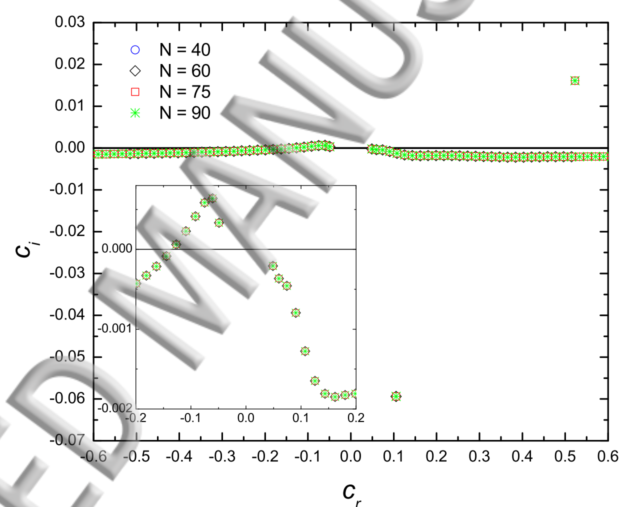

FIG. 8. Eigenvalue spectrum in the $c_r - c_i$ plane for the Carreau fluid past a deformable solid for parameters $n = 0.5$, $Re = 1000$, $H = 10$, $\Gamma_d = 0.5$, $k = 0.75$, $\lambda_d = 1$ and $\eta_\infty = 10^{-3}$. The figure confirms the convergence for different collocation points.

We next use the Carreau model to study the stability of non-Newtonian flow past the deformable surface. To establish the convergence of the eigenvalues by using the pseudo-spectral method for the present problem, we plot the spectra for different number of collocation points (N) in Fig. 8. The inset plot highlights the extent of convergence for the eigenvalues. Although the Carreau model is defined only to describe the shear thinning phenomena, it is successful in reconciling the characteristics, regardless of the way the system was non-dimensionalized. Contrary to the neutral stability curves for the power-law fluid, Fig. 9 presents a consistent trend for both the rigid and deformable scalings. Fig. 10 presents this fact showing a consistent scaling of $\Gamma \sim Re^{-\frac{1}{3}}$, where $\lambda_d = 10$ for the deformable scaling plot and $\lambda_r = 10$ for the rigid scaling plot. The variation of the critical shear-rate, Γ_c for finite Re for the Carreau fluid using a deformable scaling is shown in Fig. 11. However,

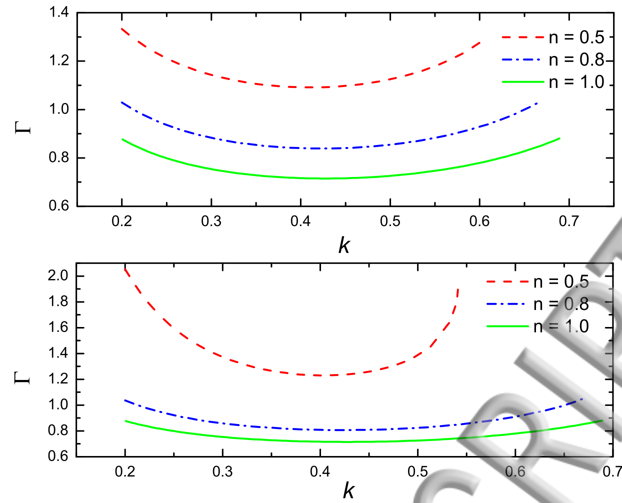

FIG. 9. Comparison of the neutral stability curves for the Carreau fluid at $H = 4$, $\eta_\infty = 0.01$ in the creeping-flow limit. The top plot depicts the rigid scaling (with $\lambda_r = 1$) and the bottom plot is for the deformable scaling (with $\lambda_d = 1$).

when λ_r is kept constant, then the base state viscosity (Eq. 12) gets immediately fixed and is independent of Re, as λ_r is a flow-dependent dimensionless group. This explains why the scaling for wall modes for a shear thinning Carreau fluid is identical to that of a Newtonian fluid. For a fixed λ_r, the fluid is effectively 'Newtonian' as the shear-rate dependence is masked by setting λ_r to a constant. As discussed in Sec. II, it is also possible to keep $\tilde{\lambda}_r$ to be constant, and this choice would allow the shear thinning nature of the fluid to play a role (see Eq. 13) in the scaling of the unstable wall modes.

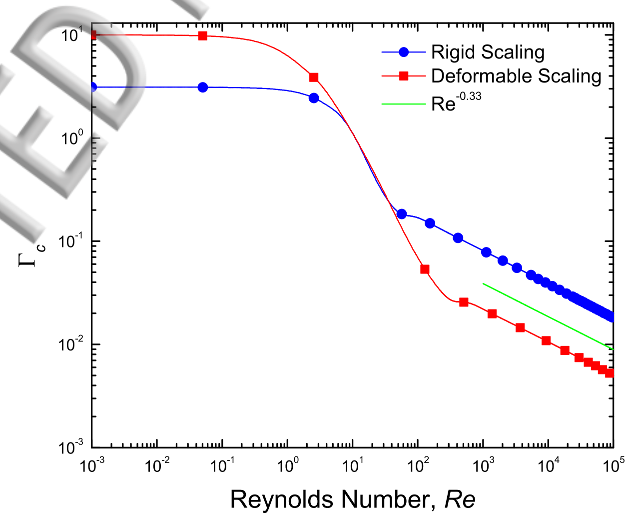

FIG. 10. Comparison of non-dimensional critical strain-rate, Γ_c as a function of Re for the rigid and deformable non-dimensional scalings for the Carreau fluid. The parameters used are $n = 0.5$, $H = 10$ and $\eta_\infty = 10^{-5}$. For rigid scaling, $\lambda_r = 10$, and for deformable scaling, $\lambda_d = 10$.

Indeed, a simple scaling argument illustrates this aspect more clearly. For unstable wall modes, we postulate (following Ref. 14) that the Newtonian wall mode scaling (Ref. 33) of

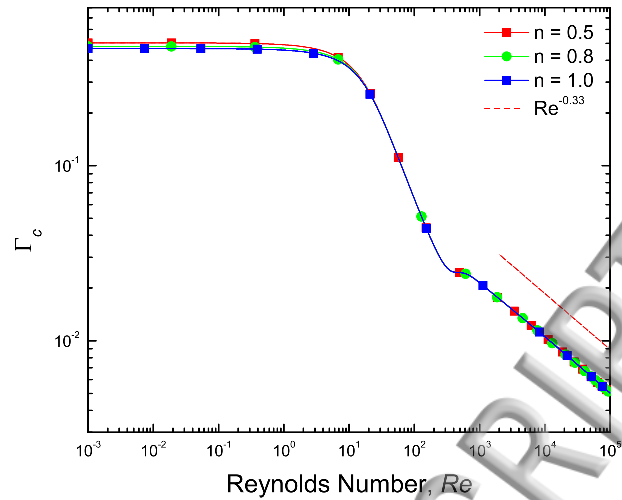

FIG. 11. Comparison of non-dimensional critical strain-rate, Γ_c as a function of Re for different n using the deformable non-dimensional scaling for the Carreau fluid. The parameters used are $\lambda_d = 1$, $\eta_\infty = 0.5$ and $H = 10$.

$\Gamma \propto Re^{-1/3}$ holds even for the shear thinning Carreau fluid, but with the viscosity in the scaling being replaced by the prevalent viscosity at the shear-rate of the base flow. This yields

$$\left(\frac{V_m^* \eta_{app}^*}{G^* R^*}\right) \sim \left(\frac{\eta_{app}^*}{\rho^* V^* R^*}\right)^{1/3} \tag{65}$$

where η_{app} is the viscosity corresponding to the prevalent shear rate in the flow. For sufficiently high shear rates, the Carreau model yields $\eta_{app}^* \sim \eta_0^*(\tilde{\lambda}_r Re)^{(n-1)}$. Upon substituting this in the above equation, and defining $\Gamma = V_m^* \eta_0^*/(G^* R^*)$ and $Re = \rho^* V_m^* R^*/\eta_0^*$ we obtain (for fixed $\tilde{\lambda}_r$)

$$\Gamma \sim Re^{\frac{(1-2n)}{3}}. \tag{66}$$

Thus, the wall mode scaling of a Carreau fluid indeed shows a dependence on the power-law index n, and a decrease in n from unity (Newtonian limit) leads to a stabilizing effect as shown by the above scaling relation. Our numerical results shown in Fig. 12 indeed conform to the above scaling argument, and at $Re \gg 1$, the scaling exponent for different n from the numerics is very close to the theoretical exponent of $(1-2n)/3$ derived above.

A. Short-wave instability

For the Carreau model, in the creeping-flow limit, we explore the short-wave instability and the criterion required for it to be realized. The short-wave instability discussed by Gaurav and Shankar[47] is realized for a finite Reynolds number at a critical Γ which is an $\mathcal{O}(1)$ quantity. The neo-Hookean solid exhibits a first normal stress difference in the base state which gives rise to a short-wave instability for $\Gamma \sim O(1)$ or higher and is convective in nature[48]. For the Carreau model, in the limit of $\eta_\infty = 0$, it is known that,

$$\eta \sim \eta_0(\lambda_d \Gamma)^{n-1}.$$

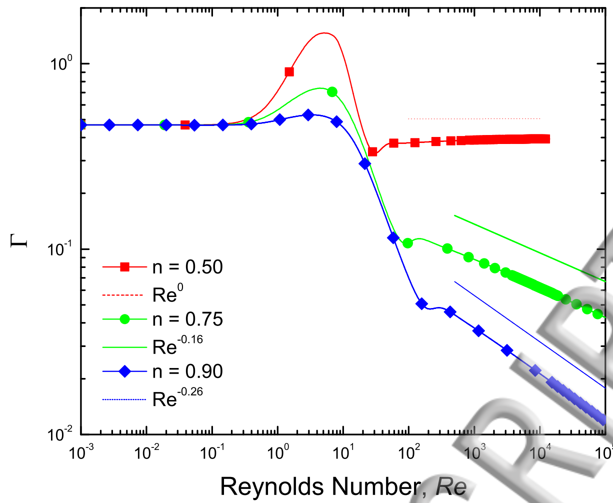

FIG. 12. Comparison of non-dimensional critical strain-rate, Γ for neutral modes as a function of Re for different n for the Carreau fluid. The parameters used are $\tilde{\lambda}_r = 1$, $k = 0.45$, $\eta_\infty = 10^{-5}$ and $H = 10$. The theoretically predicted exponents for $n = 0.5$, 0.75 and 0.9 are respectively 0, -0.167 and -0.267.

The deformable scaling is used for this mathematical reduction. Using this relation into the condition for the short-wave instability,

$$\frac{\eta_0^* V_m^*}{G^* R^*} \sim (\lambda_d \Gamma)^{1-n}.$$

Re-arranging this simplification, we obtain the relation,

$$\Gamma \sim \lambda_d^{\frac{1-n}{n}}. \tag{67}$$

Similarly, we obtain the relation for the rigid scaling, by incorporating the fact that $\lambda_r = \Gamma \lambda_d$,

$$\Gamma \sim \lambda_r^{1-n}. \tag{68}$$

We show the agreement of this theoretical analysis in Fig. 13 for the rigid scaling using a shear-rate that is neutrally stable for the system.

B. Effect of η_∞ and λ_r on the Stability

Finally, we explore the effect of the parameters of the Carreau fluid on the stability of the system. We analyze the effect of variation of the dimensionless relaxation time, λ_r on Γ_c for finite Reynolds numbers. The parameter λ_r represents the time constant at which there is a transition from the zero-shear Newtonian plateau to the power-law region. As can be seen in Fig. 14, $\lambda_r = 1$ appears to be the most unstable, while $\lambda_r = 100$ is the most stable. This could be interpreted by checking the relative position of the graphs, with a higher critical strain rate indicating that the flow is relatively stable. It has been shown in this work that for the Carreau fluid, shear-thinning has a stabilizing effect compared to the Newtonian fluid. Hence we observe that the increase in relaxation time has a stabilizing

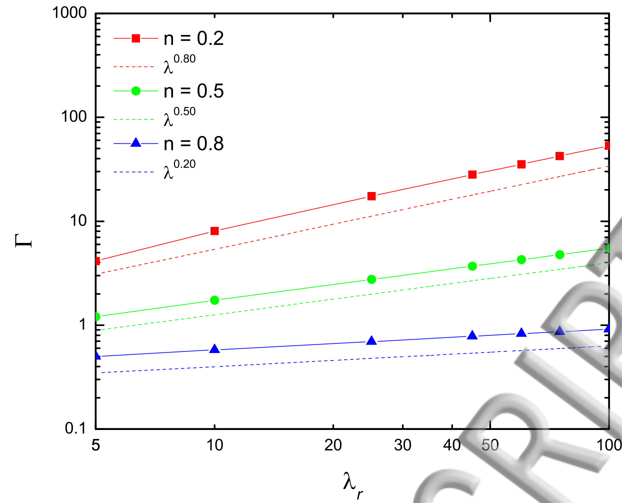

FIG. 13. Scaling of the non-dimensional strain rate, Γ, with λ_r for different values of n at $k = 0.2$ and $H = 10$ for the short-wave mode in the creeping flow limit for the Carreau fluid. The short-wave mode scales as $\Gamma \sim (\lambda_r)^{1-n}$.

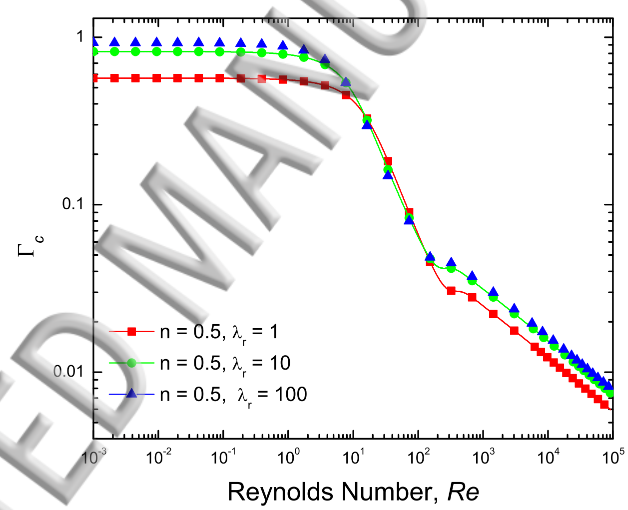

FIG. 14. Effect of the variation of λ_r on the stability for the Carreau fluid with $n = 0.5$, $H = 10$, $\eta_\infty = 0.5$ and $k = 0.45$.

effect for given values of η_0 and η_∞.

The effect of the non-dimensional infinite-shear viscosity η_∞, which characterizes the high shear-rate asymptotic value of η for the Carreau model is explored next. The role of the non-dimensional viscosity at infinite shear-rate on the stability in $\Gamma_c - Re$ plane is shown in Fig. 15. It can be seen that $\eta_\infty = 0.5$ appears to be the most unstable, whereas $\eta_\infty = 0.001$ is the most stable. A low value of η_∞ implies that the shear-thinning effect is high. As η_∞ tends to 1, the shear-thinning effect reduces, and the fluid remains Newtonian in nature. The shear-thinning fluid (for which the Carreau model is applicable) has been shown in this work to be more stable compared to the Newtonian fluid, and hence increasing the non-dimensional infinite shear-rate proves to be de-stabilizing in nature.

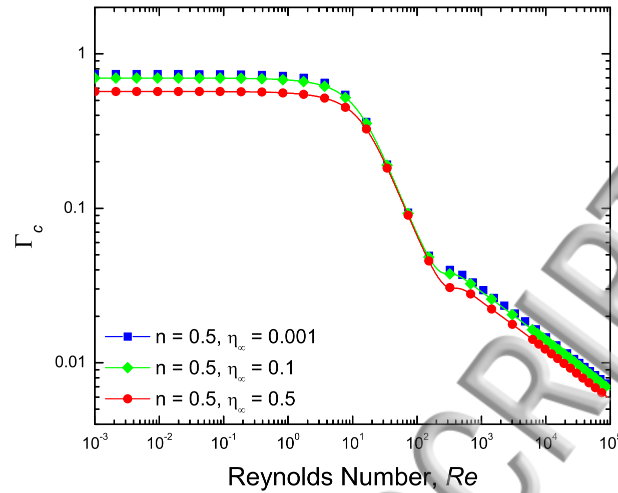

FIG. 15. Effect of the variation of η_∞ on the stability for a Carreau fluid with $n = 0.5$, $H = 10$, $\lambda_r = 1$ and $k = 0.45$.

Eigenfunctions are plotted at a high Reynolds number, Re, to depict the perturbations in the stream-wise direction for a neutrally stable eigenmode after normalizing them to unity at the interface. A sharp variation in the stream-wise velocity perturbation is seen near the fluid-solid interface which decays to zero on progression to the top wall. Similar to that observed by Roberts and Kumar[13] for the power-law fluid, we observe for the Carreau fluid in Fig. 16 that the magnitude of the perturbation in the fluid side is lesser for the shear-thinning fluid than the Newtonian case[46]. The decrease in boundary layer thickness for the shear-thickening fluids is consistent with the behavior of the power-law fluid as reported by Giribabu and Shankar[14]. It is noteworthy that even for high values of H, which indicates that the solid side is far thicker than the fluid side, a perturbation can be seen in the x-direction velocity for the solid.

IV. CONCLUSIONS

The linear stability of plane Couette flow of shear-thinning fluids past a neo-Hookean solid is analyzed using both power-law and Carreau models. The role of the shear-rate dependence of the viscosity of the fluid on the instabilities in flow past a deformable solid is explored in this work. For the power-law model, an algebraic discrepancy in the formulation of the previous studies is corrected and is shown to result only in quantitative differences in the results. Because the power-law fluid does not have a proper viscosity scale, the problem is formulated using two different scalings for non-dimensionalization for the power-law fluid. The 'rigid' scaling used can be considered to be flow-dependent, while the 'deformable' scaling is material-dependent in nature. For the power-law fluid, at high Re, wall modes show a scaling of $\Gamma \sim Re^{\frac{-1}{2n+1}}$ for the deformable scaling as shown in the previous study of Giribabu and Shankar[14]. However, using the rigid scaling, wall modes show a scaling of $\Gamma \sim Re^{-\frac{1}{3}}$, independent of the power-law index, n. This apparent discrepancy is shown to arise because different quantities were set to unity in the two scalings, and with this idea, it is possible to derive one scaling from the other. However, this still does not answer the

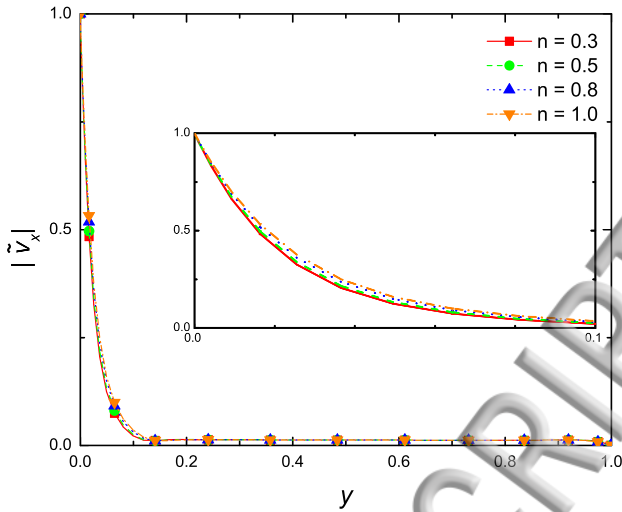

FIG. 16. Streamwise velocity eigenfunction plotted for the Carreau fluid for different values of n for the parameters: $H = 10$, $\eta_\infty = 0.5$, $\lambda_r = 1$, $\Gamma = 0.0144$, $k = 0.592$ and $Re = 3 \times 10^3$.

question of whether strength of shear thinning (as quantified by the power-law index n) plays a role on the wall mode instability.

This indeterminacy is argued to arise because of a lack of a (zero-shear) viscosity scale in the power-law model. It is not possible to discriminate between the two scaling behaviour for wall modes (obtained as a consequence of using two different schemes for non-dimensionalization) within the power-law model itself. To resolve this apparent paradox, it is necessary to use a model that exhibits a well-defined zero-shear viscosity plateau, and the Carreau model is one of the simplest models that accomplishes this. To this end, we carried out stability analysis of plane Couette flow of a Carreau fluid past a deformable solid surface. It has been shown that regardless of the scaling used for the Carreau model, when the paramter $\lambda_r = \lambda^* V_m^*/R^*$ is fixed, for high Re, $\Gamma \sim Re^{-\frac{1}{3}}$, which has been previously seen for the Newtonian case[33]. The invariance in the scaling exponent arises because when λ_r is fixed, the shear thinning nature of the fluid viscosity gets masked. To circumvent this, a flow-independent dimensionless group $\tilde{\lambda}_r = \lambda^* \eta_0^*/(\rho^* R^{*2})$ is fixed, and this results in the unstable wall modes to scale as $\Gamma \sim Re^{\frac{(1-2n)}{3}}$. This scaling behaviour was shown to arise out of a simple argument that the Newtonian wall mode scaling is applicable for a Carreau fluid with the viscosity being interpreted as the viscosity prevalent at the shear rate of the base flow. This scaling behaviour is also confirmed from our numerical results. The role of the parameters of the Carreau model on the stability of the system is investigated. A parametric sweep showed that the increase in η_∞ de-stabilizes the system while an increase in λ is stabilizing to the system. Thus, we show that the shear-thinning fluid is more stable compared to the Newtonian fluid using the Carreau model. An analysis for the short-wave instability in the limit of creeping flow and $\eta_\infty = 0$, showed a relation of $\Gamma \sim (\lambda_d)^{\frac{1-n}{n}}$ for the deformable scaling, and a relation of $\Gamma \sim (\lambda_r)^{1-n}$ for the rigid scaling.

The present study thus unambiguously demonstrates, using the Carreau model, that shear-rate dependent viscosity has a stabilizing effect on the instabilties present in flow past a deformable solid surface both at low and high Re. This stabilization due to shear thinning is in marked contrast with the experimental results of Srinivas and Kumaran[29] which showed that the consequence of polymer addition led to destabilization of the instability present in a

Newtonian fluid. It is useful to estimate the dimensionless parameters in the experiments[29]: the channel half width used was $\sim 100\mu$m, elasticity modulus of the wall was 18kPa, the relaxation time of the polymer solution was ~ 1 ms, flow velocities are in the range of 5ms^{-1}. Thus $Re \sim 100$ in their experiments, and the nondimensional solid elastic modulus $\Gamma \sim 0.002$. These values are similar to the regimes in which instability is predicted in the present theoretical study (see Figures 10 and 11). While an Oldroyd-B model qualitatively predicts the destabiliation, it does not predict a change in the scaling exponent in the Γ-Re relation. Thus, it appears that in order for an accurate description of the experimental results, both elasticity and shear-thinning nature of the polymer solution must be taken into account. This could be achieved, perhaps, with the use of a White-Metzner model with Carreau model for viscosity variation with shear rate, and such models could be used in future theoretrical efforts. The predictions of this study will be relevant to the flow of dilute and semi-dilute polymer solutions, especially in microscale flows, past deformable solid surfaces. In particular, such instabilities may be potentially exploited in the enhancement of mixing in the flow of polymer solutions in microfluidic applications.

REFERENCES

[1] J. B. Grotberg and O. E. Jensen, "Biofluid mechanics in flexible tubes," Ann. Rev. Fluid Mech. **36**, 121–147 (2004).
[2] T. M. Squires and S. R. Quake, "Microfluidics: Fluid physics at the nanoliter scale," Rev. Mod. Phys. **77**, 977–1026 (2005).
[3] P. Krindel and A. Silberberg, "Flow through gel-walled tubes," J. Colloid Interface Sci. **71**, 34–50 (1979).
[4] V. Kumaran, "Experimental studies on the flow through soft tubes and channels," Sadhana **40**, 911–923 (2015).
[5] V. Shankar, "Stability of fluid flow through deformable tubes and channels: An overview," Sadhana **40**, 925–943 (2015).
[6] M. A. Unger, H.-P. Chou, T. Thorsen, A. Scherer, and S. R. Quake, "Monolithic microfabricated valves and pumps by multilayer soft lithography," Science **288**, 113–116 (2000).
[7] N. L. Jeon, D. T. Chiu, C. J. Wargo, H. Wu, I. S. Choi, J. R. Anderson, and G. M. Whitesides, "Microfluidics section: Design and fabrication of integrated passive valves and pumps for flexible polymer 3-dimensional microfluidic systems," Biomedical Microdevices **4**, 117–121 (2002).
[8] V. Shankar and S. Kumar, "Instability of viscoelastic plane Couette flow past a deformable wall," Journal of Non-Newtonian Fluid Mechanics **116**, 371 – 393 (2004).
[9] A. Kumar and V. Shankar, "Instability of high-frequency modes in viscoelastic plane Couette flow past a deformable wall at low and finite Reynolds number," Journal of Non-Newtonian Fluid Mechanics **125**, 121 – 141 (2005).
[10] P. Chokshi and V. Kumaran, "Stability of the viscous flow of a polymeric fluid past a flexible surface," Physics of Fluids **19**, 034102 (2007).
[11] P. Chokshi and V. Kumaran, "Stability of the flow of a viscoelastic fluid past a deformable surface in the low Reynolds number limit," Phys. Fluids **19**, 104103 (2007).
[12] P. Chokshi, P. Bhade, and V. Kumaran, "Wall-mode instability in plane shear flow of viscoelastic fluid over a deformable solid," Phys. Rev. E **91**, 023007 (2015).
[13] S. A. Roberts and S. Kumar, "Stability of creeping Couette flow of a power-law fluid past a deformable solid," J. Non-Newtonian Fluid Mech. **139**, 93–102 (2006).

[14]D. Giribabu and V. Shankar, "Stability of plane Couette flow of a power-law fluid past a neo-Hookean solid at arbitrary Reynolds number," Phys. Fluids **29**, 074106 (2017).
[15]P. J. Carreau, "Rheological equations from molecular network theories," Transactions of the Society of Rheology **16**, 99–127 (1972).
[16]R. G. Larson, *Constitutive Equations for Polymer Melts and Solutions* (Butterworths, Boston, 1988).
[17]R. B. Bird, R. C. Armstrong, and O. Hassager, *Dynamics of Polymeric liquids, Vol 1 Fluid Mechanics*, 2nd ed. (Wiley-Interscience, New York, 1987).
[18]C. Nouar and I. Frigaard, "Stability of plane CouettePoiseuille flow of shear-thinning fluid," Physics of Fluids **21**, 064104 (2009).
[19]V. Gkanis and S. Kumar, "Instability of creeping Couette flow past a neo-Hookean solid," Phys. Fluids **15**, 2864–2471 (2003).
[20]V. Kumaran, "Stability of the viscous flow of a fluid through a flexible tube," J. Fluid Mech. **294**, 259–281 (1995).
[21]V. Kumaran, "Stability of the flow of a fluid through a flexible tube at intermediate Reynolds number," J. Fluid Mech. **357**, 123–140 (1998).
[22]V. Shankar and V. Kumaran, "Stability of non-parabolic flow in a flexible tube," J. Fluid Mech. **395**, 211–236 (1999).
[23]V. Shankar and V. Kumaran, "Stability of fluid flow in a flexible tube to non-axisymmetric disturbances," J. Fluid Mech. **407**, 291–314 (2000).
[24]R. Thaokar, V. Shankar, and V. Kumaran, "Effect of tangential interface motion on the viscous instability in fluid flow past flexible surfaces," European Physical Journal B - Condensed Matter and Complex Systems **23**, 533–550 (2001).
[25]L. E. Malvern, *Introduction to the Mechanics of a Continuous Medium* (Prentice-Hall, Englewood Cliffs, NJ, 1969).
[26]V. Kumaran, "Stability of the flow of a fluid through a flexible tube at high Reynolds number," J. Fluid Mech. **302**, 117–139 (1995).
[27]Gaurav and V. Shankar, "Stability of fluid flow through deformable neo-Hookean tubes," Journal of Fluid Mechanics **627**, 291322 (2009).
[28]R. Patne, D. Giribabu, and V. Shankar, "Consistent formulations for stability of fluid flow through deformable channels and tubes," Journal of Fluid Mechanics **827**, 3166 (2017).
[29]S. S. Srinivas and V. Kumaran, "Effect of viscoelasticity on the soft-wall transition and turbulence in a microchannel," Journal of Fluid Mechanics **812**, 10761118 (2017).
[30]V. Gorodtsov and A. Leonov, "On a linear instability of a plane parallel Couette flow of viscoelastic fluid," Journal of Applied Mathematics and Mechanics **31**, 310 – 319 (1967).
[31]V. Kumaran, G. Fredrickson, and P. Pincus, "Flow induced instability of the interface between a fluid and a gel at low Reynolds number," J. Phys. II France **4**, 893–911 (1994).
[32]A. S. Kumar and V. Shankar, "Instability of high-frequency modes in viscoelastic plane Couette flow past a deformable wall at low and finite Reynolds number," J. Non-Newtonian Fluid Mech **125**, 121–141 (2005).
[33]V. Shankar and V. Kumaran, "Asymptotic analysis of wall modes in a flexible tube revisited," Euro. Phys. J. B. **19**, 607–622 (2001).
[34]V. Kumaran, "Asymptotic analysis of wall modes in a flexible tube," Euro. Phys. J. B. **4**, 519–527 (1998).
[35]M. Pourjafar, H. Hamedi, and K. Sadeghy, "Stability of power-law fluids in creeping plane Poiseuille: The effect of wall compliance," Journal of Non-Newtonian Fluid Mechanics **216**, 22 – 30 (2015).

[36]M. Pourjafar and K. Sadeghy, "Linear stability of shear-thinning fluids in deformable channels: Effect of inertial terms," Journal of Non-Newtonian Fluid Mechanics **230**, 80 – 91 (2016).

[37]M. K. S. Verma and V. Kumaran, "A multifold reduction in the transition Reynolds number, and ultra-fast mixing, in a micro-channel due to a dynamical instability induced by a soft wall," J. Fluid Mech. **727**, 407–455 (2013).

[38]R. Neelamegam and V. Shankar, "Experimental study of the instability of laminar flow in a tube with deformable walls," Phys. Fluids **27**, 024102 (2015).

[39]Gaurav and V. Shankar, "Stability of pressure-driven flow in a deformable neo-Hookean channel," J. Fluid Mech. **659**, 318–350 (2010).

[40]D. Giribabu and V. Shankar, "Consistent formulation of solid dissipative effects in stability analysis of flow past a deformable solid," Phys. Rev. Fluids **1**, 033602 (2016).

[41]R. Patne, D. Giribabu, and V. Shankar, "Consistent formulations for stability of fluid flow through deformable channels and tubes," Journal of Fluid Mechanics **827**, 3166 (2017).

[42]P. Chokshi and V. Kumaran, "Weakly nonlinear analysis of viscous instability in flow past a neo-Hookean surface," Phys. Rev. E **77**, 056303 (2008).

[43]R. Liu and Q. Liu, "Non-modal instabilities of two-dimensional disturbances in plane Couette flow of a power-law fluid," Journal of Non-Newtonian Fluid Mechanics **165**, 1228 – 1240 (2010).

[44]J. A. Weideman and S. C. Reddy, "A Matlab differentiation matrix suite," ACM Trans. Math. Software **26**, 465–519 (2000).

[45]V. Shankar and V. Kumaran, "Stability of fluid flow in a flexible tube to non-axisymmetric disturbances," Journal of Fluid Mechanics **407**, 291314 (2000).

[46]V. Shankar and V. Kumaran, "Stability of wall modes in fluid flow past a flexible surface," Physics of Fluids **14**, 2324–2338 (2002).

[47]Gaurav and V. Shankar, "Stability of fluid flow through deformable neo-Hookean tubes," J. Fluid Mech. **627**, 291–322 (2009).

[48]R. Patne and V. Shankar, "Absolute and convective instabilities in combined Couette-Poiseuille flow past a neo-Hookean solid," Physics of Fluids **29**, 124104 (2017).

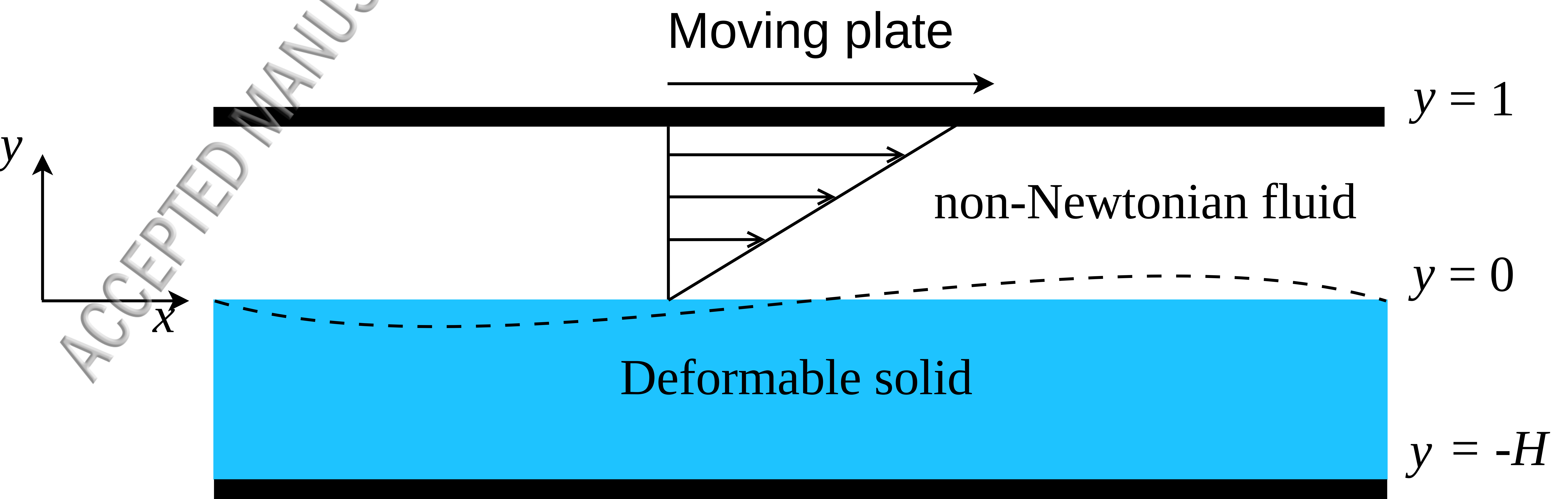
Moving plate
y = 1
y
non-Newtonian fluid
y = 0
x
Deformable solid
y = -H

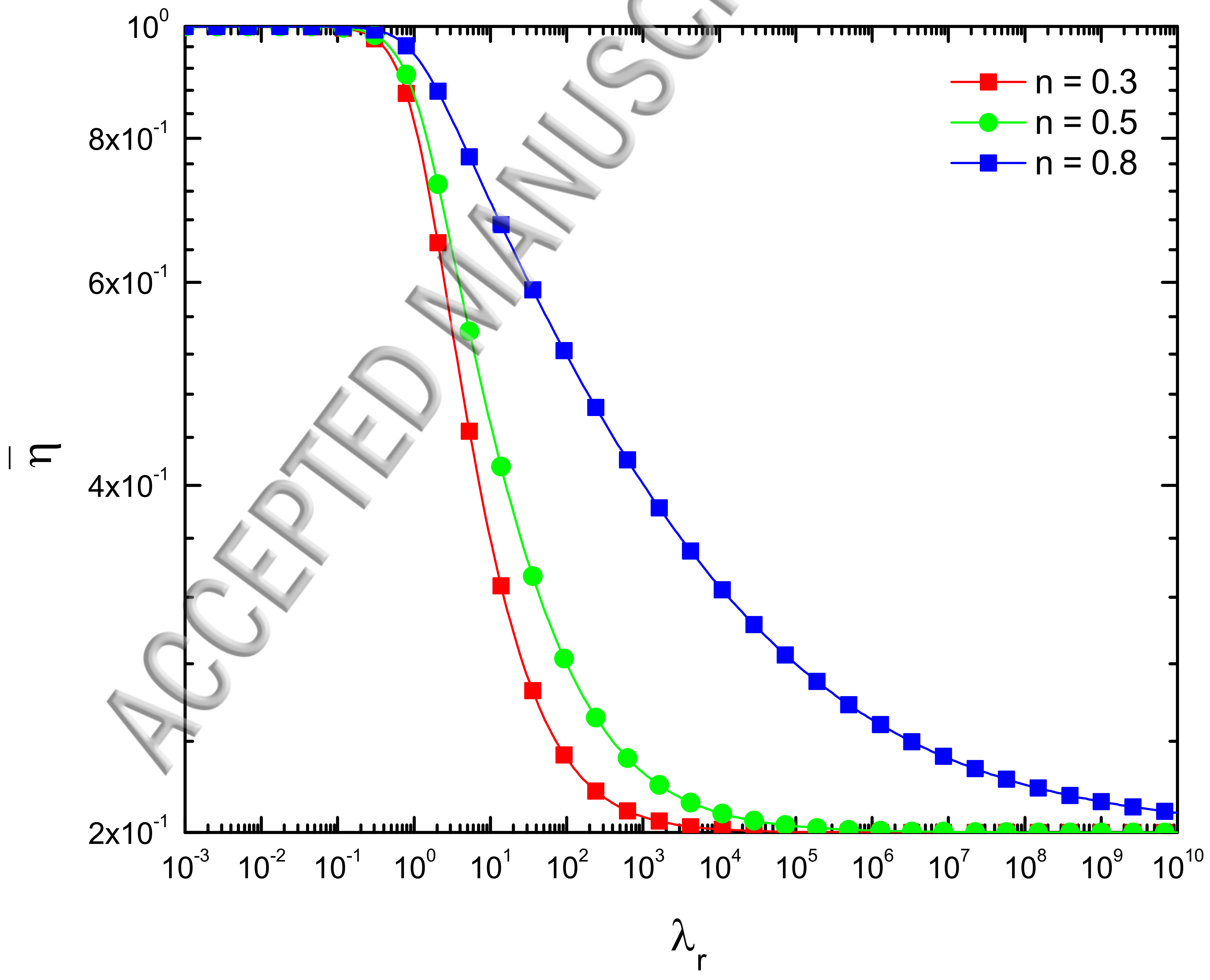

n = 0.3
n = 0.5
n = 0.8
10^0
$8x10^{-1}$
$6x10^{-1}$
$4x10^{-1}$
$2x10^{-1}$
$\bar{\eta}$
10^{-3} 10^{-2} 10^{-1} 10^0 10^1 10^2 10^3 10^4 10^5 10^6 10^7 10^8 10^9 10^{10}
λ_r

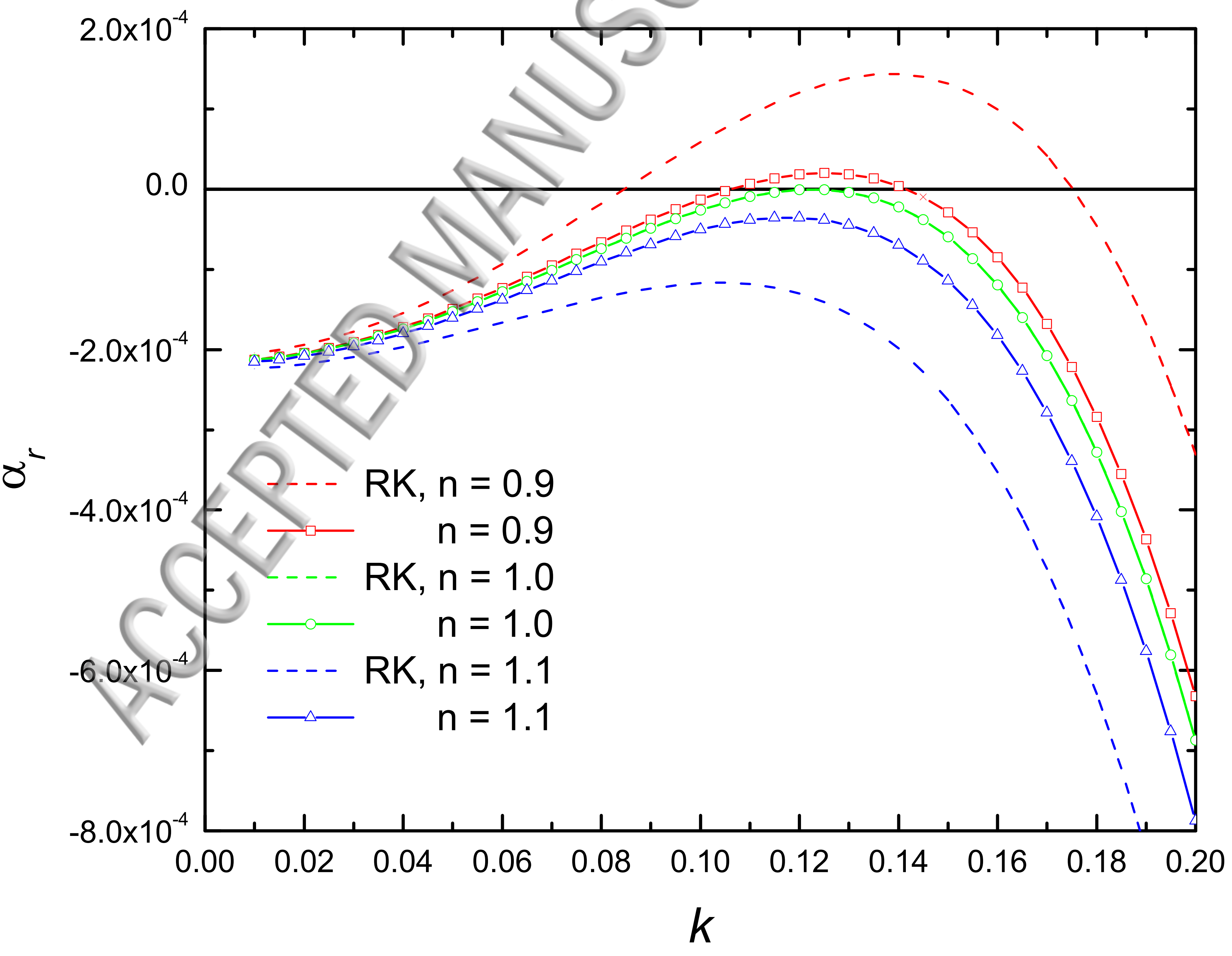

2.0x10-4
0.0
-2.0x10-4
-4.0x10-4
-6.0x10-4
-8.0x10-4
0.00
0.02
0.04
0.06
0.08
0.10
0.12
0.14
0.16
0.18
0.20
αr
k
RK, n = 0.9
n = 0.9
RK, n = 1.0
n = 1.0
RK, n = 1.1
n = 1.1

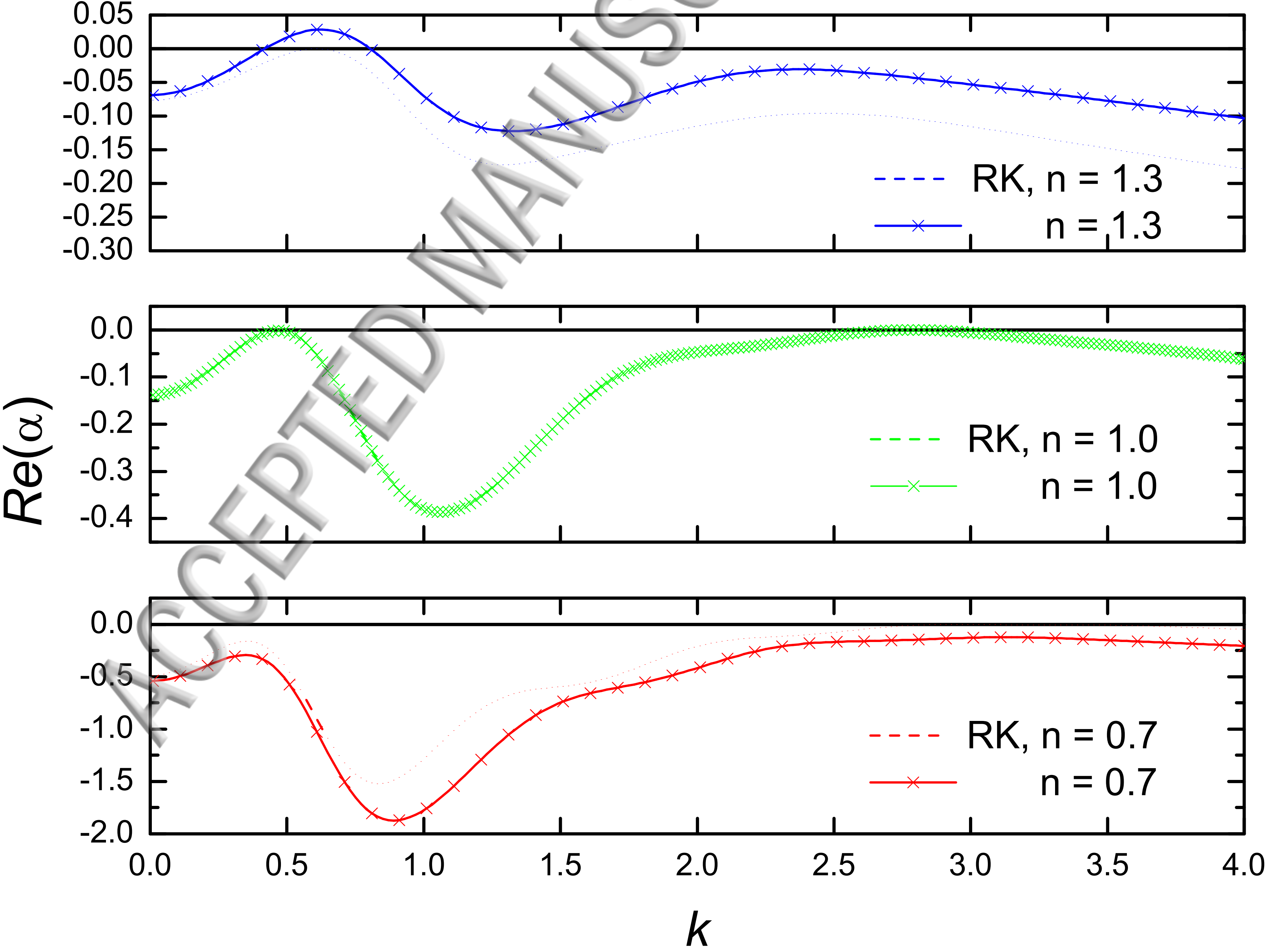

RK, n = 1.3
n = 1.3
RK, n = 1.0
n = 1.0
RK, n = 0.7
n = 0.7
Re(α)
k

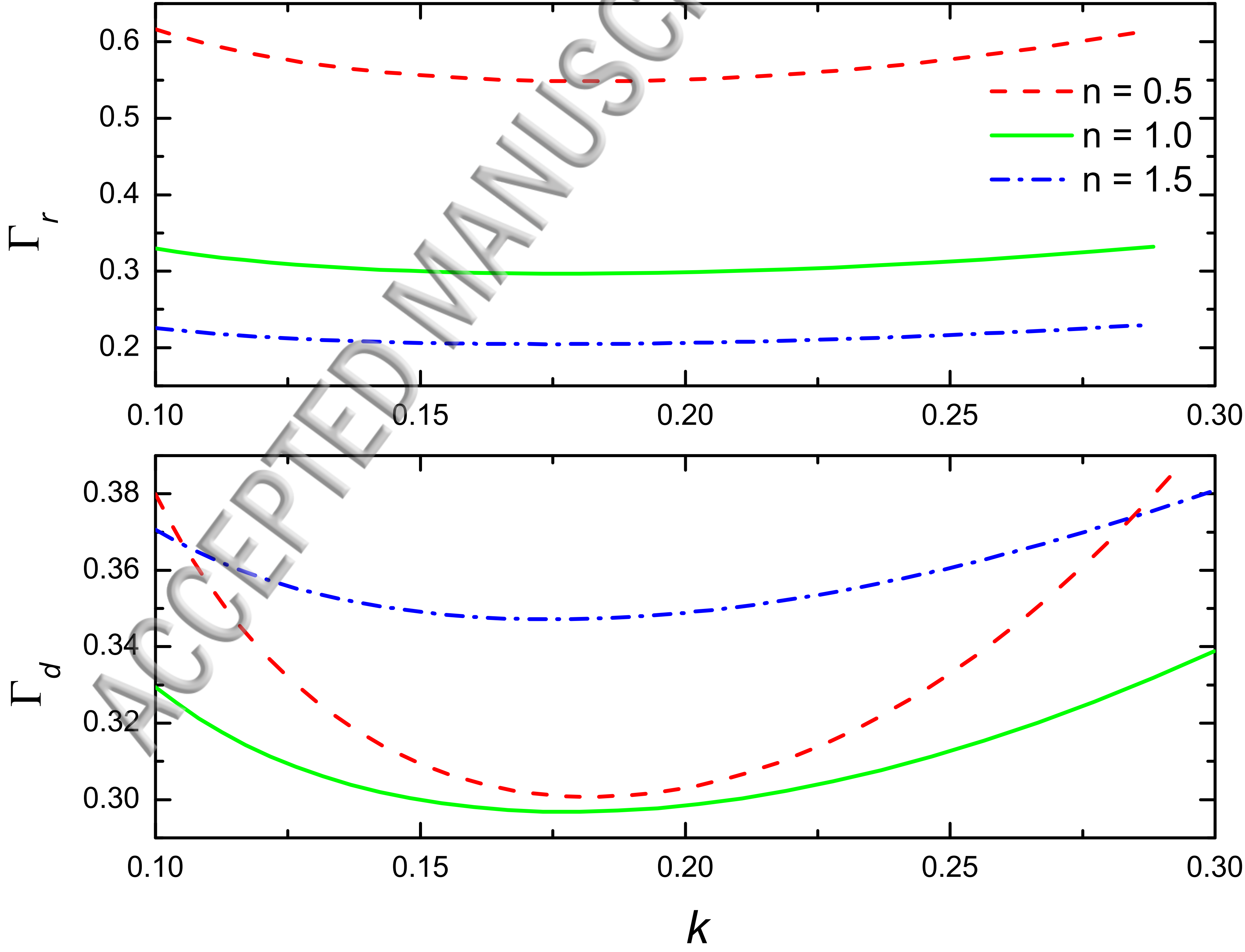

n = 0.5
n = 1.0
n = 1.5
Γ_r
Γ_d
0.2
0.3
0.4
0.5
0.6
0.30
0.32
0.34
0.36
0.38
0.10
0.15
0.20
0.25
0.30
k

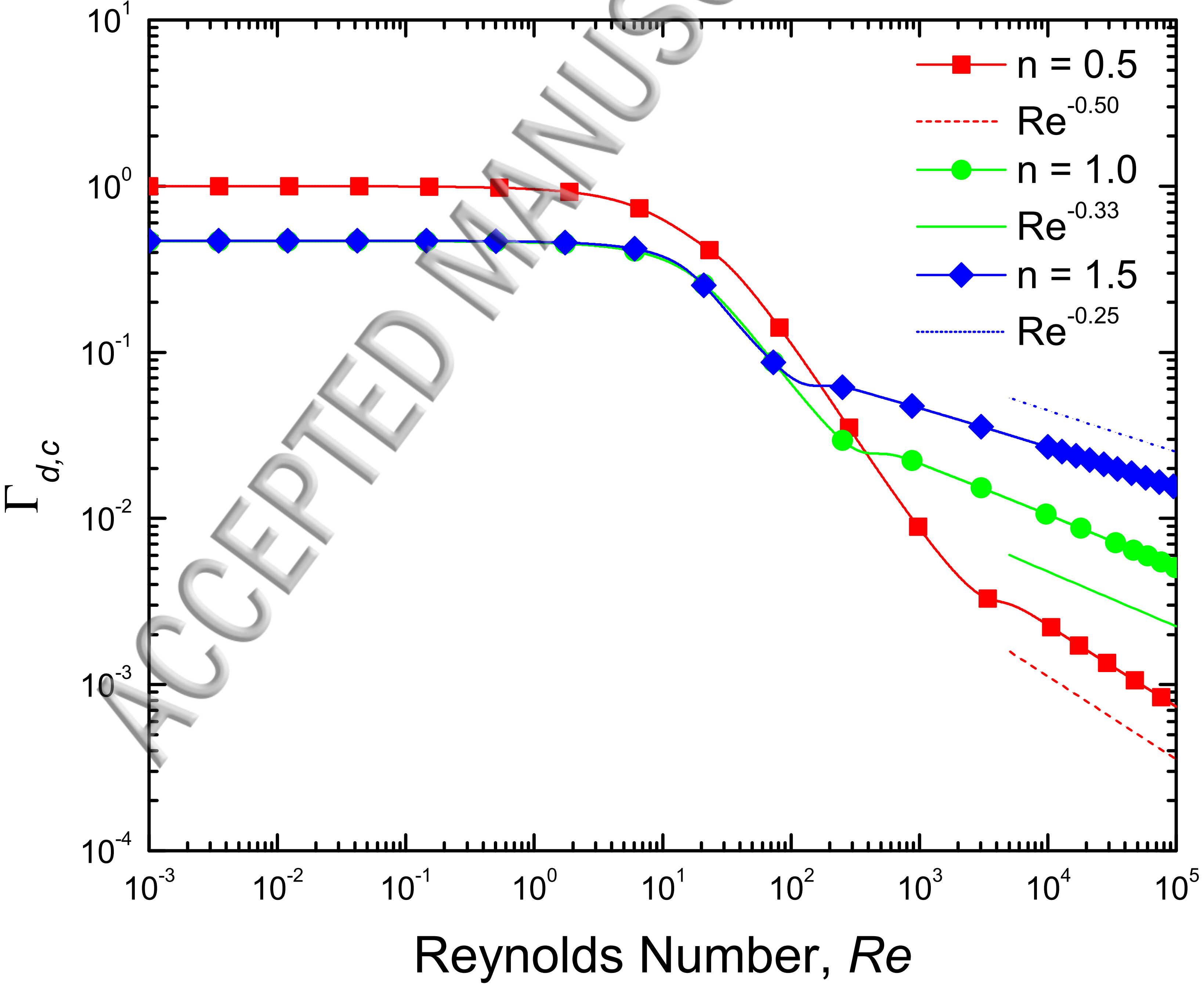

n = 0.5
Re-0.50
n = 1.0
Re-0.33
n = 1.5
Re-0.25
Γd,c
Reynolds Number, Re

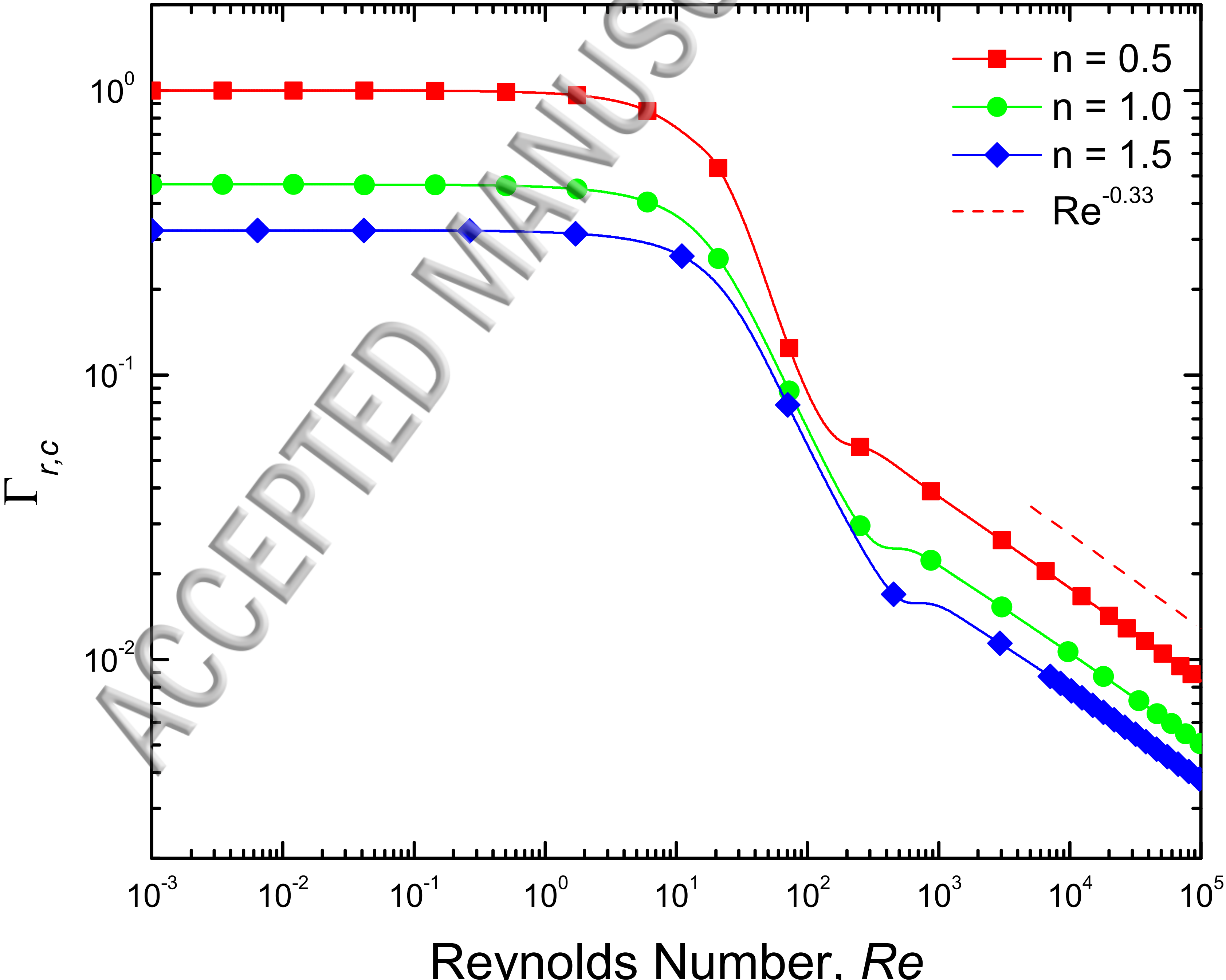

n = 0.5
n = 1.0
n = 1.5
Re^-0.33
10^0
10^{-1}
10^{-2}
$\Gamma_{r,c}$
10^{-3} 10^{-2} 10^{-1} 10^0 10^1 10^2 10^3 10^4 10^5
Reynolds Number, *Re*

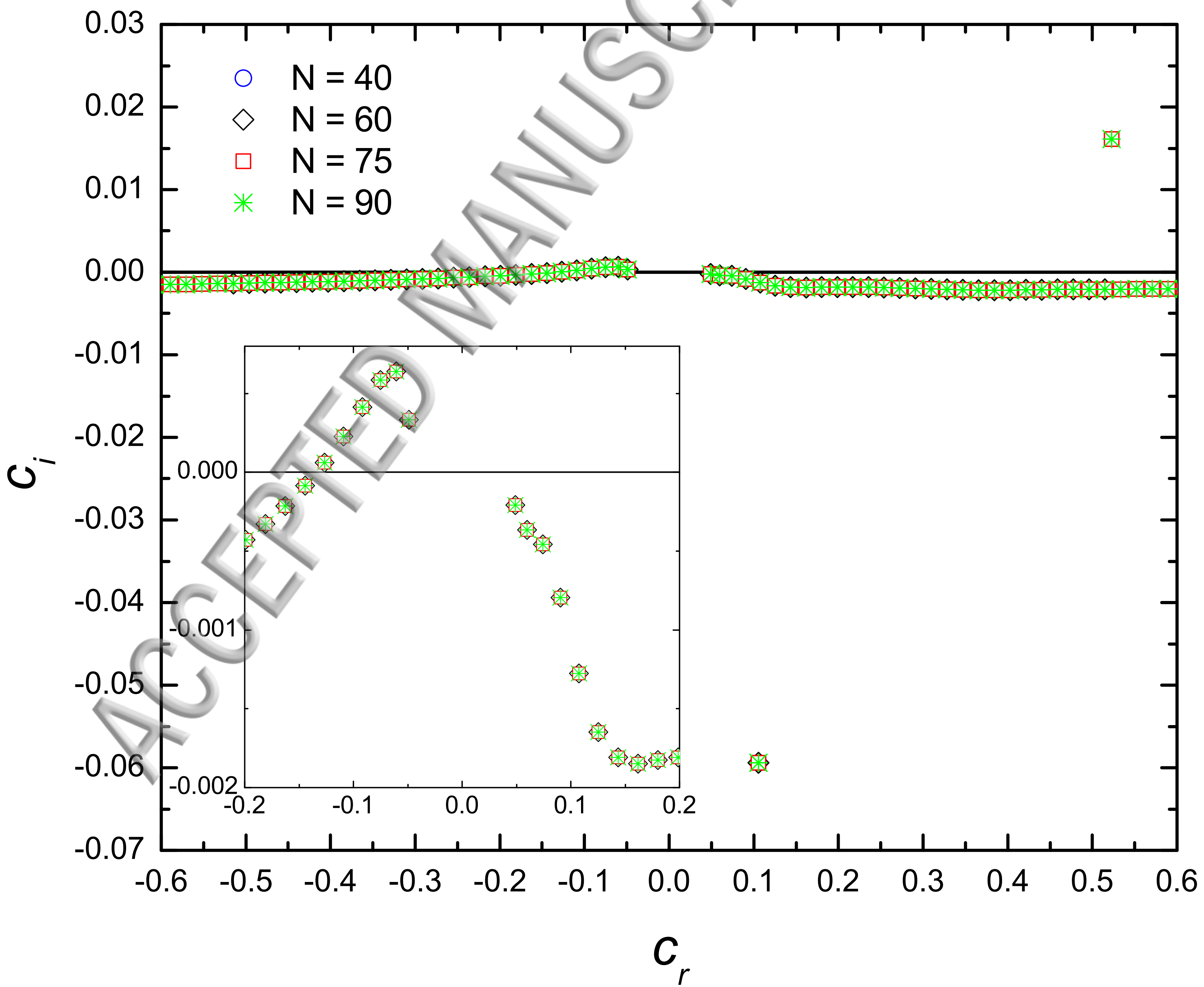

N = 40
N = 60
N = 75
N = 90
c_i
c_r
0.03
0.02
0.01
0.00
-0.01
-0.02
-0.03
-0.04
-0.05
-0.06
-0.07
-0.6
-0.5
-0.4
-0.3
-0.2
-0.1
0.0
0.1
0.2
0.3
0.4
0.5
0.6
0.000
-0.001
-0.002

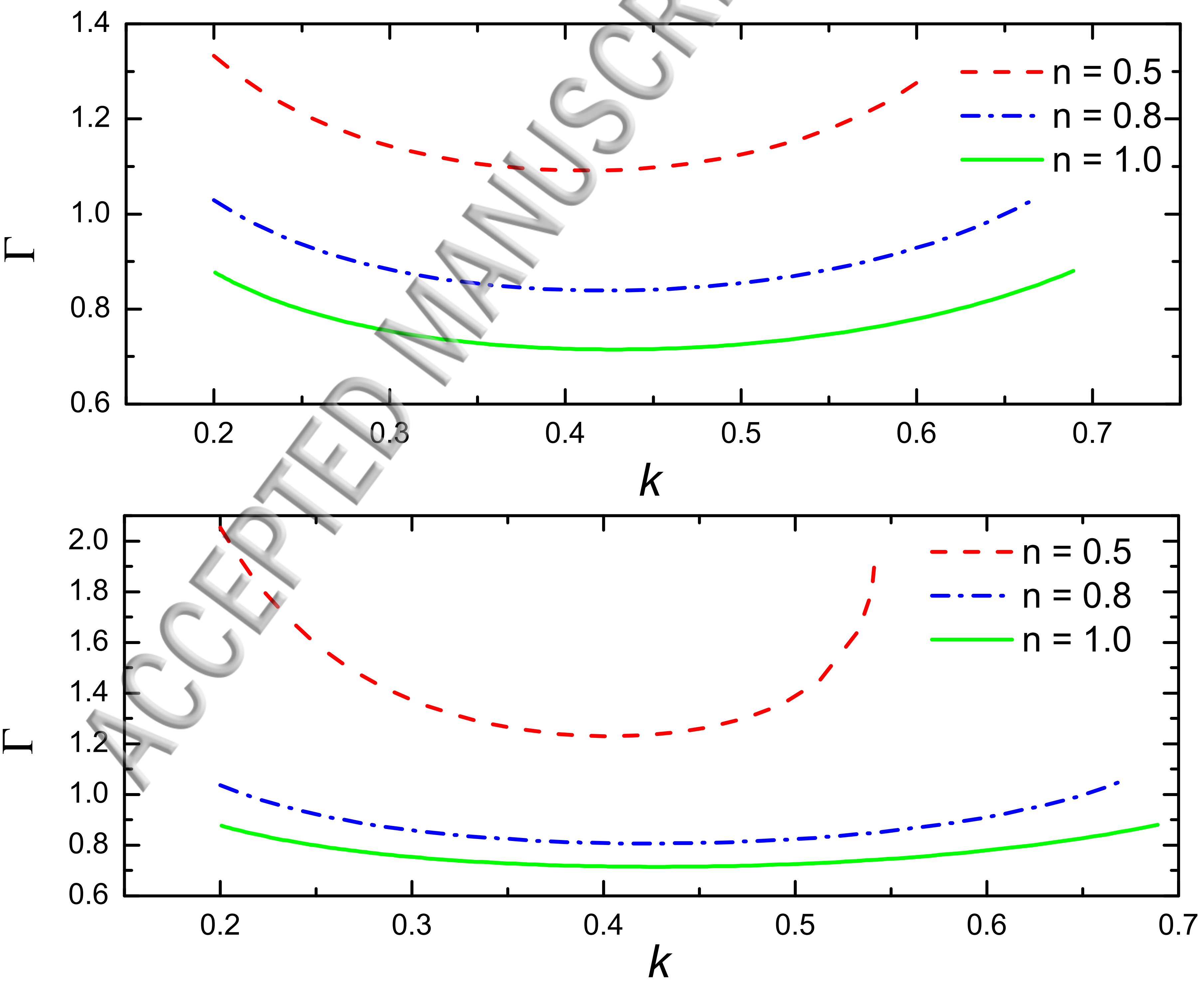
n = 0.5
n = 0.8
n = 1.0
Γ
k
0.2
0.3
0.4
0.5
0.6
0.7
0.6
0.8
1.0
1.2
1.4
1.6
1.8
2.0

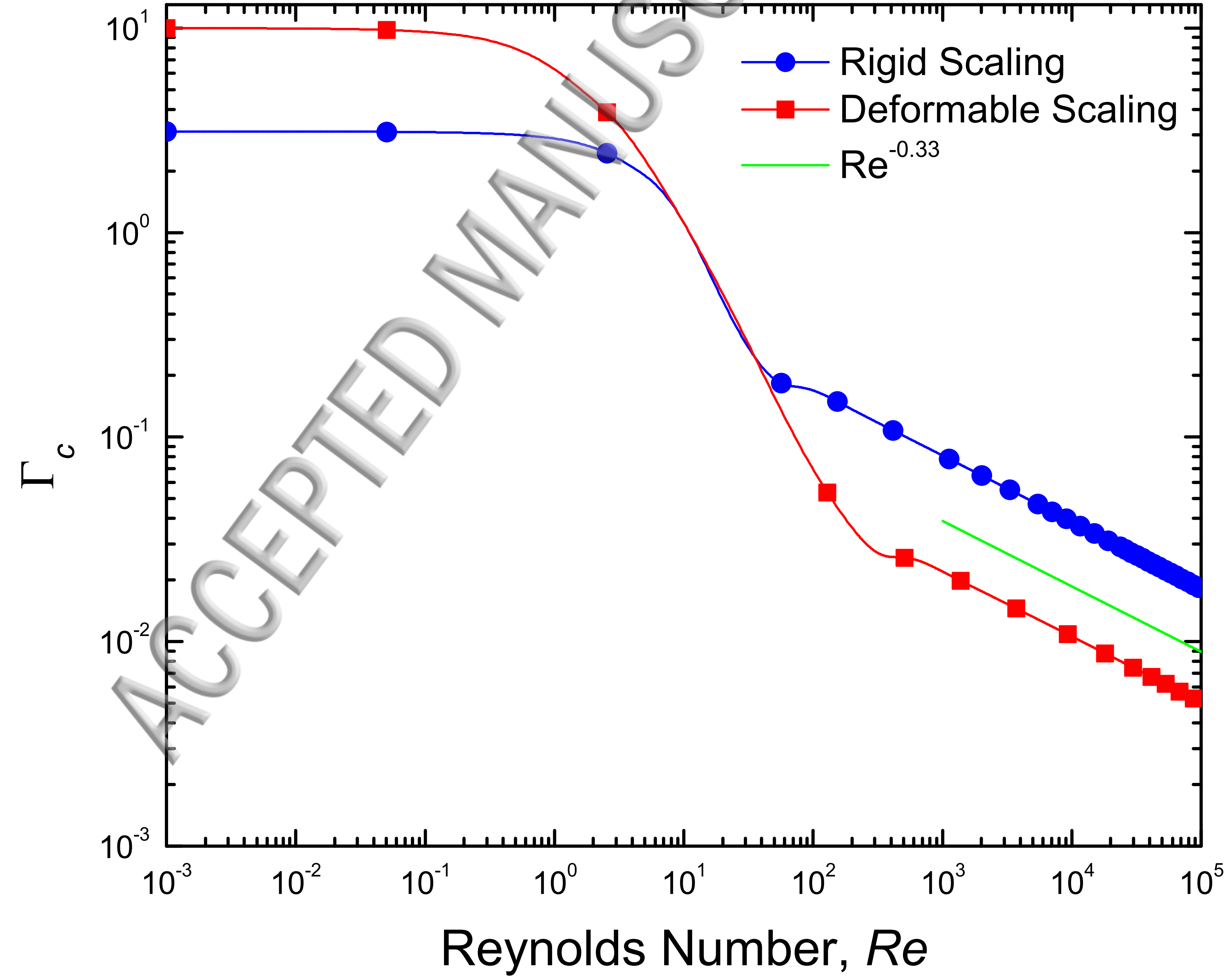

Rigid Scaling
Deformable Scaling
$Re^{-0.33}$
Γ_c
10^{1}
10^{0}
10^{-1}
10^{-2}
10^{-3}
10^{-3}
10^{-2}
10^{-1}
10^{0}
10^{1}
10^{2}
10^{3}
10^{4}
10^{5}
Reynolds Number, *Re*

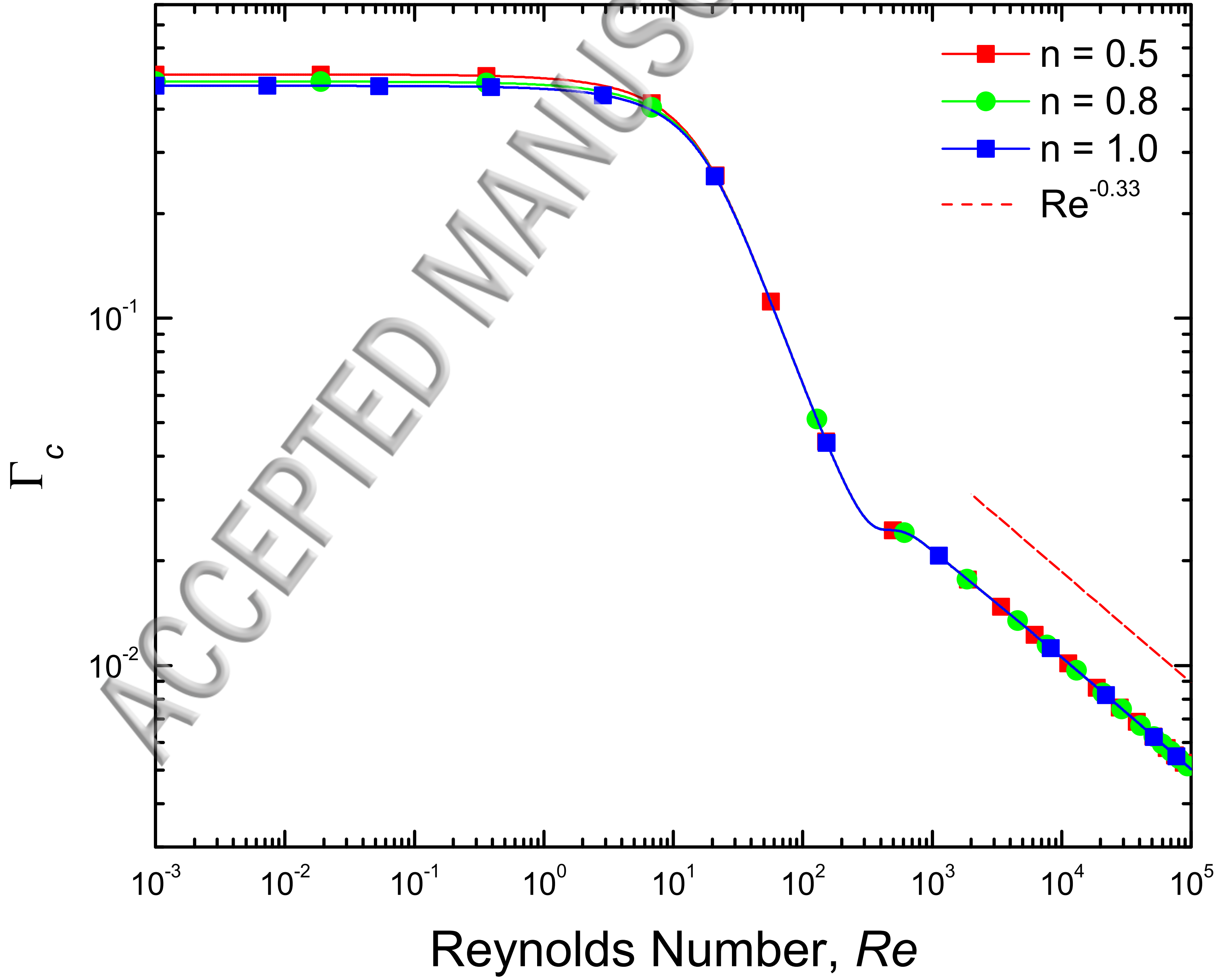

n = 0.5
n = 0.8
n = 1.0
Re^-0.33
10^-1
10^-2
Γ_c
10^-3
10^-2
10^-1
10^0
10^1
10^2
10^3
10^4
10^5
Reynolds Number, Re

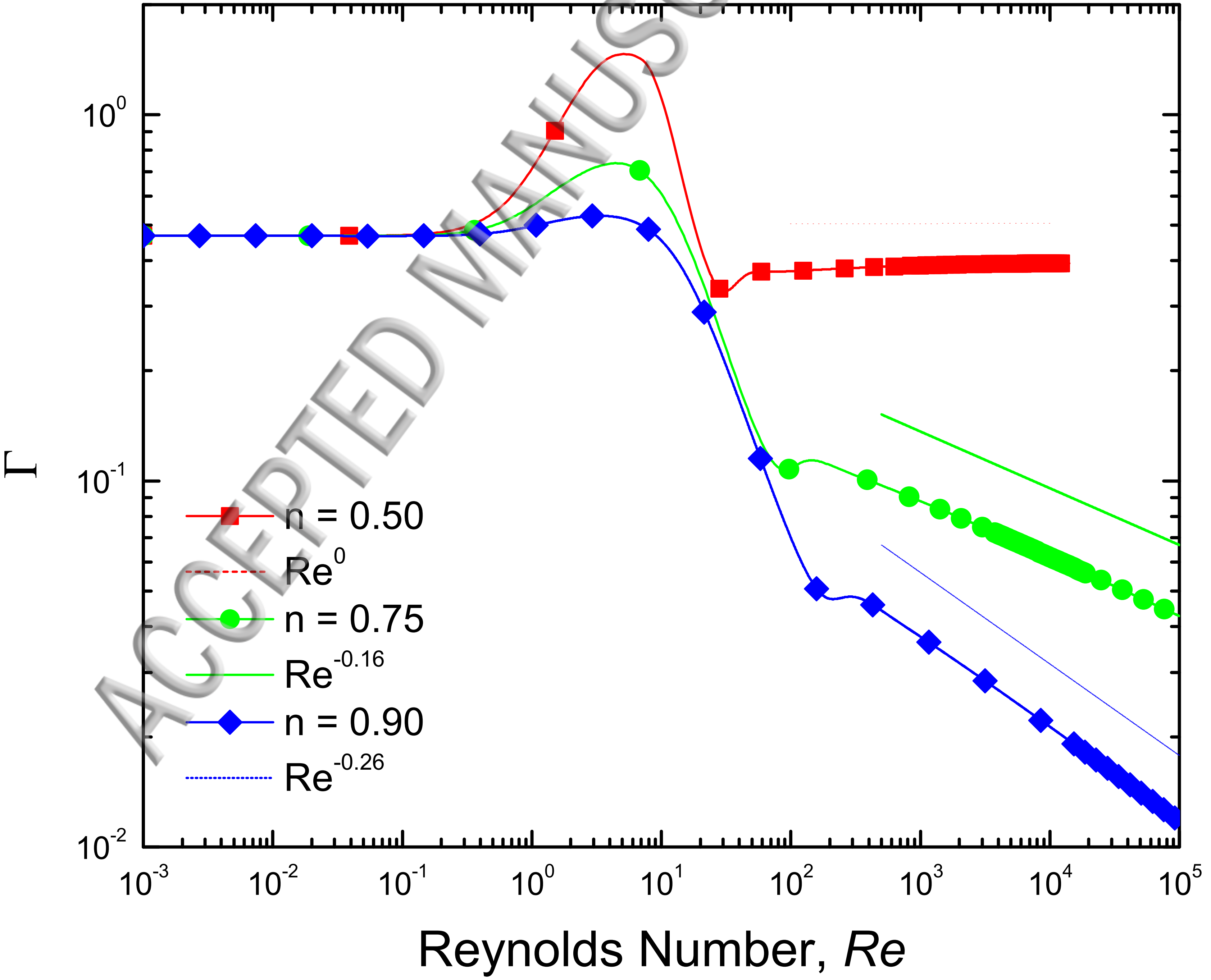

Γ
10^0
10^-1
10^-2
10^-3
10^-2
10^-1
10^0
10^1
10^2
10^3
10^4
10^5
Reynolds Number, Re
n = 0.50
Re^0
n = 0.75
Re^-0.16
n = 0.90
Re^-0.26

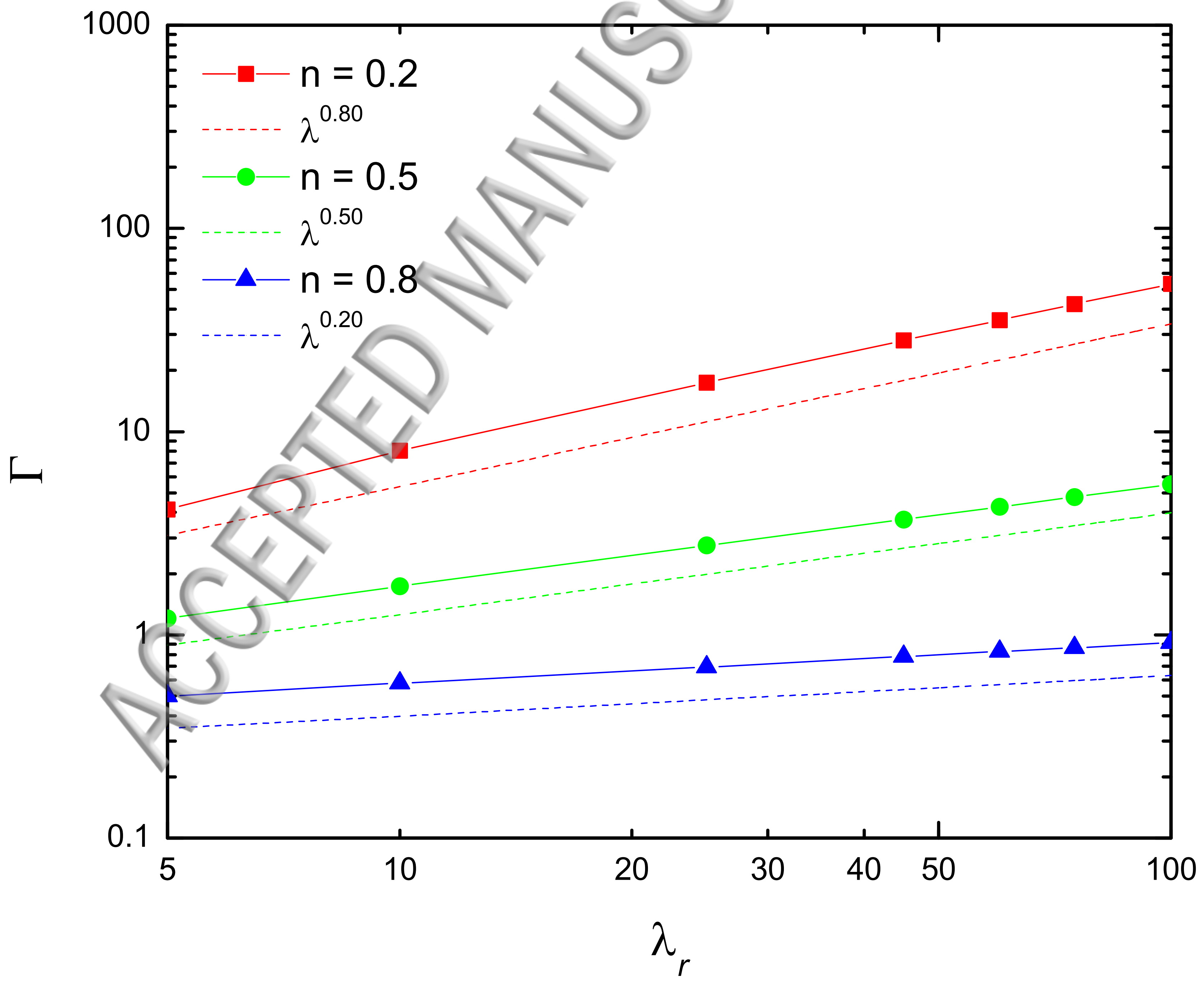

n = 0.2
$\lambda^{0.80}$
n = 0.5
$\lambda^{0.50}$
n = 0.8
$\lambda^{0.20}$
1000
100
10
1
0.1
Γ
5
10
20
30
40
50
100
λ_r

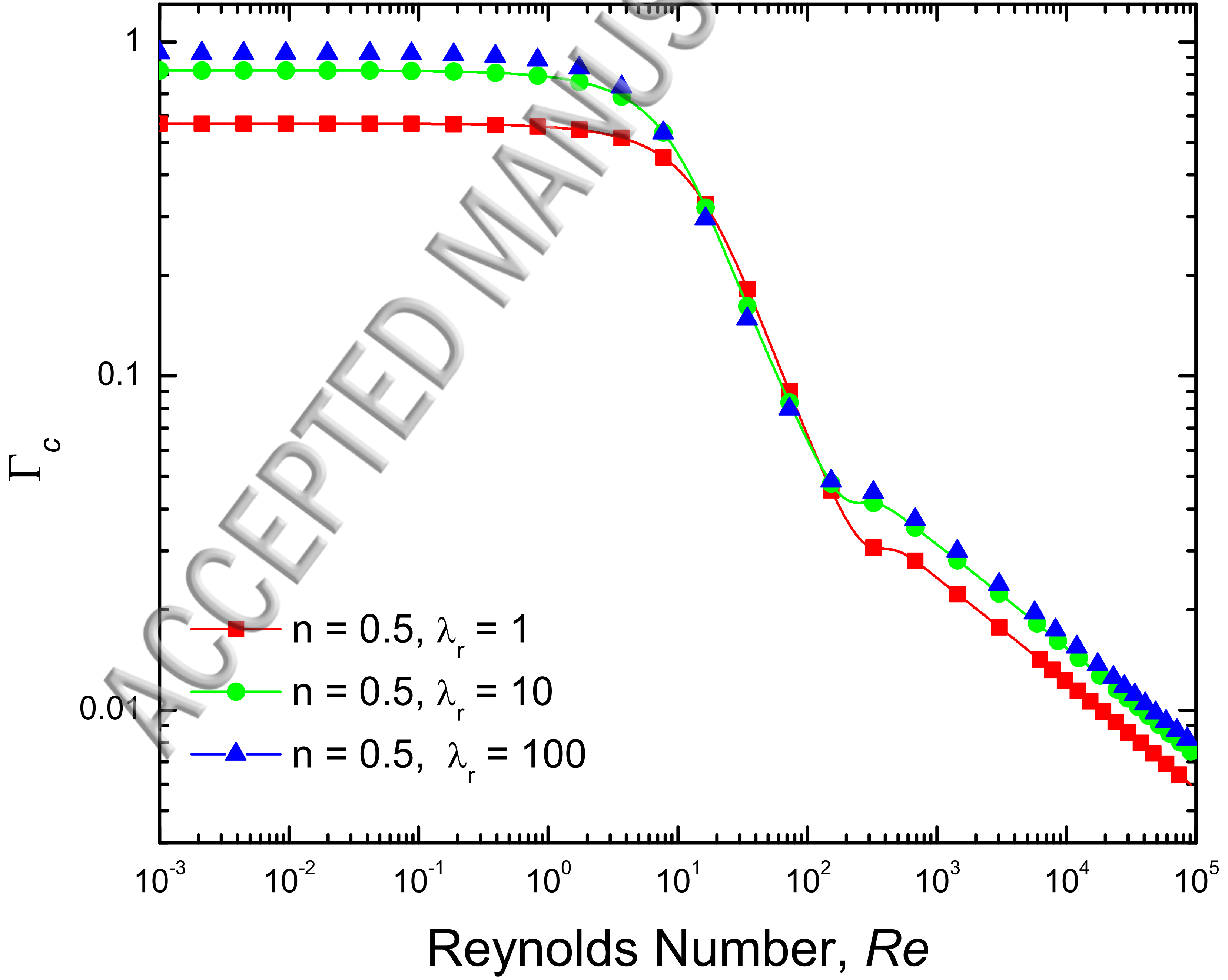

1
0.1
0.01
Γ_c
10^{-3}
10^{-2}
10^{-1}
10^{0}
10^{1}
10^{2}
10^{3}
10^{4}
10^{5}
Reynolds Number, *Re*
n = 0.5, λ_r = 1
n = 0.5, λ_r = 10
n = 0.5, λ_r = 100

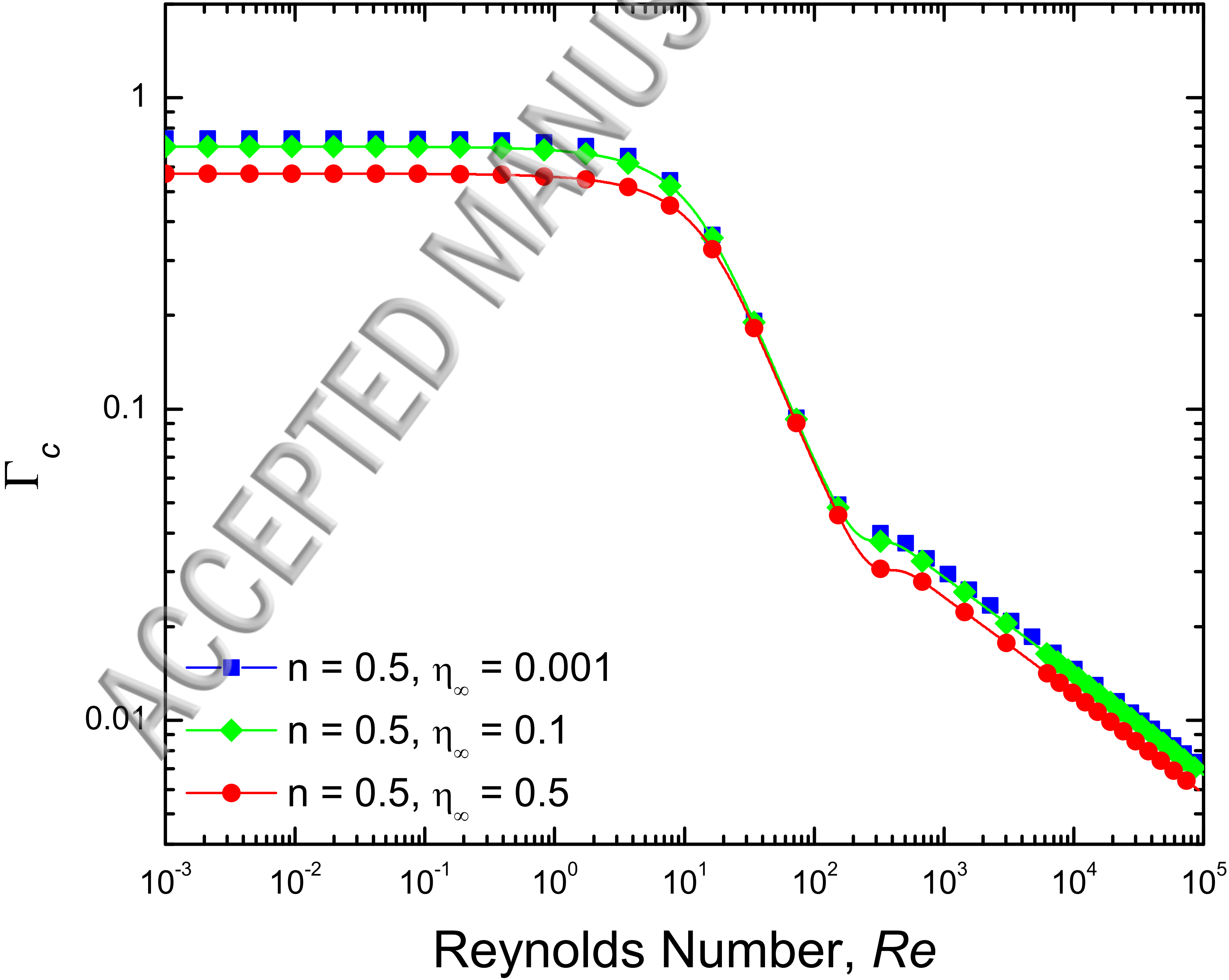

1
0.1
0.01
Γ_c
10^{-3}
10^{-2}
10^{-1}
10^{0}
10^{1}
10^{2}
10^{3}
10^{4}
10^{5}
Reynolds Number, *Re*
n = 0.5, η_∞ = 0.001
n = 0.5, η_∞ = 0.1
n = 0.5, η_∞ = 0.5

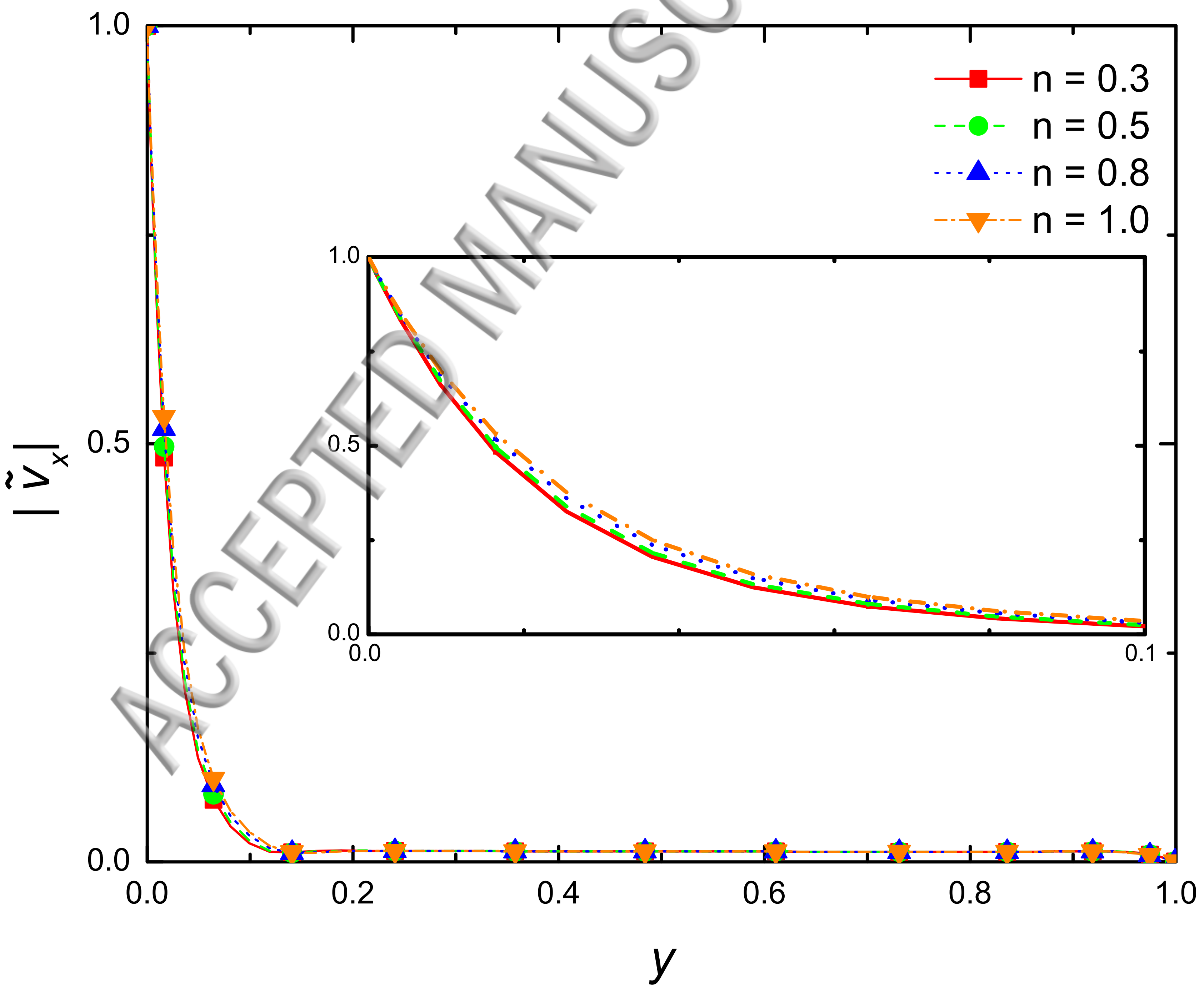

n = 0.3
n = 0.5
n = 0.8
n = 1.0
$|\tilde{v}_x|$
y
0.0
0.2
0.4
0.6
0.8
1.0
0.5
0.1